参赛学生姓名：姜艺霖

中学：上海星河湾双语学校

省份：上海市

国家/地区：中国

指导老师姓名：阮振超、陈昌斌

指导老师单位：上海星河湾双语学校、中国科学院上海药物研究所

论文题目：Mycendin-1: AI-Assisted Discovery and Experimental Characterization of a Novel Antifungal Peptide

2026 S.-T. Yau High School Science Award
仅用于2026丘成桐中学科学奖公文公示

Mycendin-1: AI-Assisted Discovery and Experimental Characterization of a Novel Antifungal Peptide

Yilin Jiang

Abstract

Invasive fungal infections remain difficult to treat because of limited antifungal diversity, toxicity, resistance, and biofilm-associated tolerance. Here, an AI-assisted generation and screening workflow nominated five candidate antifungal peptides, from which Mycendin-1 (MCD-1) was selected for experimental evaluation. MCD-1 showed antifungal activity against five of six fungal isolates, with marked species- and strain-dependent differences. Against *Candida albicans* SC5314, MCD-1 suppressed planktonic growth, reduced viable-cell counts, strongly inhibited biofilm formation, and decreased mature-biofilm metabolic activity by up to 86%. Checkerboard analysis with amphotericin B yielded a minimum fractional inhibitory concentration index of 0.125, providing evidence of synergy. In a *Galleria mellonella* infection model, MCD-1-treated larvae showed 95% survival at day 7, compared with 50% in the infected control group. Circular-dichroism spectroscopy, electron microscopy, and molecular-dynamics simulation were consistent with environment-dependent conformational adaptation, fungal-envelope perturbation, and persistent association at the membrane-water interface. These findings identify MCD-1 as a promising antifungal-peptide candidate and support further investigation of its molecular target, mammalian safety, in vivo stability, and efficacy in mammalian infection models.

Keywords: antifungal peptide; *Candida albicans*; artificial intelligence; fungal biofilm; molecular dynamics

2026 S.-T. Yau High School Science Award
仅用于2026丘成桐中学科学奖论文公示

Table of Contents

Abstract 2

1. Introduction 5

2. Materials and Methods 7

2.1 AI-assisted peptide design and computational screening 7
2.1.1 Dataset construction and candidate generation 7
2.1.2 In silico screening and lead selection 7
2.1.3 Structural prediction 7

2.2 Peptide synthesis and preparation 7

2.3 Fungal strains and culture conditions 7

2.4 Antifungal susceptibility testing 8

2.5 Growth-kinetics and Time-Kill assays 8

2.6 Antibiofilm activity 9
2.6.1 Inhibition of biofilm formation 9
2.6.2 Activity against mature biofilms 9

2.7 Checkerboard interaction assay 9

2.8 In vivo activity in *Galleria mellonella* 10

2.9 Circular-dichroism spectroscopy 10

2.10 Morphological and ultrastructural characterization 10

2.11 Molecular Dynamics Simulation of Peptide–Fungal Membrane Interactions 11

2.12 Statistical analysis 11

3. Results 12

3.1 AI-Assisted screening identifies a promising AFP candidate 12

3.2 MCD-1 exhibits species- and strain-dependent antifungal activity 13

3.3 MCD-1 suppresses planktonic fungal growth 15

3.4 MCD-1 inhibits biofilm formation 16

3.5 MCD-1 reduces the metabolic activity of mature biofilms 16

3.6 Checkerboard analysis indicates a preliminary synergistic interaction between MCD-1 and amphotericin B 17

3.7 Circular dichroism reveals solvent-dependent conformational plasticity 18

3.8 MCD-1 increases survival in a *Galleria mellonella* infection model 19

3.9 Electron microscopy reveals peptide-induced cellular and membrane damage 20

2026 S.T. Yau High School Science Award
仅用于2026丘成桐中学科学奖论文公示

3.10 Molecular-dynamics simulations reveal persistent interfacial association of MCD-1 with a fungal-membrane model 21
4. Discussion 27
4.1 Principal Findings 27
4.2 Antifungal and Antibiofilm Potential of the Lead Peptide 28
4.3 Potential for Combination Antifungal Therapy 29
4.4 Proposed Membrane-Disruption Mechanism 29
4.5 In Vivo Relevance 30
4.6 Limitations and Future Directions 31
References 32
Acknowledgements 35

2026 S. -T. Yau High School Science Award
仅用于2026丘成桐中学科学奖论文公示

1. Introduction

Fungal infections impose a substantial global public health burden. Recent epidemiological estimates indicate that invasive fungal diseases afflict roughly 6.5 million individuals each year, contributing to 3.8 million deaths, of which 2.5 million are directly attributable to fungal etiology.[1] Clinical outcomes are especially poor in immunocompromised populations, critically ill patients, and transplant recipients, where invasive infections may exhibit rapid disease progression.[1] In response to this growing threat, the World Health Organization (WHO) released its inaugural Fungal Priority Pathogens List in 2022.[2] This report categorized *Candida albicans*, *Candida auris*, *Cryptococcus neoformans*, and *Aspergillus fumigatus* into the critical-priority group and underscored an urgent demand for accelerated research and development of novel antifungal therapeutics.[2] Of these high-risk pathogens, *Candida albicans* stands as a leading etiological agent of invasive candidiasis.[3] It can switch between planktonic and biofilm-associated lifestyles, enabling persistent colonization and sustained infection across heterogeneous host microenvironments.[4]

Despite the heavy clinical burden imposed by fungal diseases, available antifungal therapies are markedly more limited than bacterial treatments. Accordingly, invasive fungal infections are primarily managed with a handful of conventional antifungal families, including azoles, echinocandins, and polyenes.[5] These agents interfere with ergosterol biosynthesis, fungal cell-wall synthesis, and membrane sterols, respectively, yet each drug class bears notable drawbacks. Amphotericin B possesses potent broad-spectrum antifungal activity but exhibits severe toxicity; azoles readily develop resistance via target-site modification and efflux pump overexpression; and echinocandins, despite lower resistance prevalence, are not exempt from resistance emergences.[5,6] As highlighted by the CDC (Centers for Disease Control and Prevention, USA), toxicity, poor drug accessibility, high cost, together with complexities in dosing and treatment regimens, constitute major barriers to current antifungal therapy.[7]

Antifungal resistance represents an additional clinical challenge, yet its prevalence varies markedly across fungal species and drug classes.[6,8] In the case of *Candida albicans*, recent global surveillance covering 6,342 clinical isolates from 41 countries demonstrated that susceptibility to echinocandins and amphotericin B remained higher than 99%, whereas azole susceptibility exhibited substantial inter-strain variability together with gradual temporal shifts.[8] Consequently, clinical management becomes highly constrained when standard therapy fails, given compounding obstacles including drug-related toxicity, biofilm-associated phenotypic recalcitrance, and the risk of emerging or geographically localized resistance, which drastically narrows therapeutic options.[6,9] The rising threat of resistant WHO-priority fungal pathogens further underscores the requirement for new antifungal agents that operate via mechanisms distinct from existing conventional therapeutics.[2,6]

Antifungal peptides (AFPs) constitute a promising approach for realizing such mechanistic diversity. AFPs are bioactive peptides that inhibit or kill fungal pathogens by targeting the fungal cell wall, plasma membrane, or intracellular components. Their key physicochemical traits, including net positive charge, hydrophobicity and amphipathic structure, promote interactions with microbial outer envelopes and endow modes-of-action distinct from classical small-molecule antifungals.[10] Multiple pre-clinical studies have demonstrated the therapeutic potential of AFPs. Li et al. constructed dendritic AFPs active against drug-resistant *Candida albicans* and

2026 Si-Tu Yan Hui School Science Award 仅用于2026思慧科学奖公示

fungal biofilms; their lead peptide, C4-3RP, exhibited protease stability, low toxicity, and in-vivo efficacy in a murine skin-infection model.[11] Analogously, Agarwal et al. characterized the 15-residue peptide SA-XV, which suppressed *Fusarium* and *Candida*, disrupted biofilms, targeted fungal membranes, and mitigated in-vivo fungal burden.[12] Cumulatively, these works illustrate that peptide-derived antifungals can integrate direct antifungal potency and antibiofilm capacity, by developing mechanisms that differ from established antifungal drug scaffolds.[10,11,12]

However, the vast combinatorial diversity of amino-acid sequences renders conventional peptide discovery extremely inefficient, as only a tiny fraction of the entire sequence space is experimentally tractable for synthesis and functional screening. Artificial intelligence (AI) offers a powerful solution to constrain this immense search space by learning latent sequence-function relationships and generating peptide candidates with predefined bioactive profiles prior to experimental validation. A list of recent studies has validated the feasibility and superiority of this AI-driven strategy. Wang et al. established a latent diffusion-based pipeline for the de novo generation of antimicrobial peptides, wherein 40 computationally prioritized sequences were subjected to experimental verification. Among these candidates, 25 exhibited potent antibacterial or antifungal activity. Notably, the lead peptide AMP-29 displayed selective inhibitory activity against *Nakaseomyces glabratus* and achieved robust therapeutic efficacy in a murine infection model.[13] However, few AI-generated antifungal peptides have been evaluated against biofilms, in combination with conventional antifungals, or in vivo.

Against this background, the present study experimentally evaluates an antifungal peptide nominated through an AI-assisted screening workflow. We sought to determine whether MCD-1 exhibited reproducible activity across planktonic growth, biofilm formation, mature biofilms, combination treatment, and an in vivo infection model, and whether its biological effects were consistent with membrane-interfacial activity, rather than evaluating activity through a single susceptibility endpoint.

The lead peptide was provisionally named Mycendin-1 (MCD-1), from Greek *mykēs*, and *-din*, defend. We hypothesized that MCD-1 would act as a membrane-interfacial antifungal peptide, inhibit planktonic and biofilm growth, and show synergistic potential with amphotericin B. The specific objectives were to (i) determine the antifungal spectrum and planktonic activity of MCD-1, (ii) evaluate its effects on biofilm formation and mature biofilms, (iii) assess its interaction with amphotericin B, (iv) examine its in vivo activity in a *Galleria mellonella* infection model, and (v) characterize its conformational plasticity and membrane-association behavior.

This study primarily addresses the limited diversity of antifungal scaffolds and the poor antibiofilm performance of current agents, while providing a foundation for future toxicity and resistance studies. By connecting computational peptide discovery with experimental and mechanistic validation, this study demonstrates how AI-guided molecular design may help expand the currently restricted antifungal-development pipeline and accelerate the identification of structurally distinct therapeutic candidates against fungal pathogens.

2026 第二十一届 High School Science Award
仅用于2026年成都中学科学奖论文公示

2. Materials and Methods

2.1 AI-assisted peptide design and computational screening

An AI-assisted workflow integrating peptide-dataset curation, conditional sequence generation, MIC prediction, physicochemical screening, and structural prediction was used to identify candidate antifungal peptides. Reference antimicrobial-peptide sequences were collected from established peptide databases and provided as input to the EvoGen-Pep condition model.[14–19] Generated sequences were filtered and evaluated using an MIC-prediction model.[20] The highest-ranked candidates subsequently underwent pepADMET-based physicochemical and toxicity screening, after which MCD-1 was selected as the lead peptide for structural prediction and experimental evaluation.[21]

2.1.1 Dataset construction and candidate generation

AI-assisted sequence-generation workflow produced the AFP sequences. Before generating the sequences, a target product profile of synthetically accessible peptides with a positive net charge, moderate hydrophobicity, predicted aqueous solubility, low aggregation potential, and low predicted hemolytic or cytotoxic activity was defined. Sequences were standardized using the single-letter amino-acid code and AlphaFold 3 was used subsequently for structural prediction.[22]

2.1.2 In silico screening and lead selection

The predicted candidates were evaluated using pepADMET.[21] Calculated descriptors included sequence length, molecular weight, net charge, charge density, isoelectric point, instability index, aromaticity, aliphatic index, Boman index and hydrophobic-residue ratio. Predicted toxicity, cytotoxicity, hemolysis, HC_{50} and human-blood half-life were also considered where available.[21] We took MCD-1 (FCRSLRKLATWLLPTTFCAISKKC) forward for experimental evaluation following the prespecified review of these properties.

2.1.3 Structural prediction

The three-dimensional structure of the selected peptide was predicted using AlphaFold 3. Models were ranked using the confidence metrics provided by AlphaFold, including predicted local distance difference test scores and predicted aligned error where applicable.[22]

2.2 Peptide synthesis and preparation

Mycendin-1 (MCD-1; FCRSLRKLATWLLPTTFCAISKKC) was chemically synthesized by solid-phase peptide synthesis by GenScript (Nanjing, China).[23] Analytical high-performance liquid chromatography assessed peptide purity, and mass spectrometry verified molecular mass before biological testing.

2.3 Fungal strains and culture conditions

All fungal manipulations were performed in a class II biological safety cabinet (HFsafe-1200; Heal Force). YPD broth contained 10 g/L yeast extract, 20 g/L peptone, and 20 g/L glucose; 20 g/L agar was added for solid YPD. Sabouraud dextrose agar was prepared at 64 g/L and solid media were sterilized at 121 °C for 21 min. A BPH-9042 constant-temperature incubator (Shanghai Yiheng Technology) performed incubation.

2026 S.T. Yau High School Science Award
仅用于2026丘成桐中学科学奖公示

The primary experimental strain was *Candida albicans* SC5314. The secondary susceptibility panel comprised *Candida tropicalis* 93, *Candida tropicalis* 305, *Nakaseomyces glabratus* 310, *Cryptococcus* sp. 909, and *Cryptococcus* sp. 994. All strains were obtained from the host laboratory collection and handled in an institutionally approved biosafety level 2 laboratory.

Frozen stocks were streaked onto yeast extract–peptone–dextrose agar and incubated at 30 °C for approximately 48 h to obtain isolated colonies. For each experiment, a single colony was inoculated into 5 mL YPD broth and cultured at 30 °C with shaking at 200 rpm for approximately 16 h.

For long-term storage, 900 μL of an overnight culture was mixed with 900 μL of sterile 50% glycerol and stored at −80 °C in a Panasonic MDF-U539-C medical freezer. Cultures were pelleted when required using an Eppendorf 5810R centrifuge or a Himac CT15RE refrigerated high-speed centrifuge.

2.4 Antifungal susceptibility testing

Fluconazole (PHR1160-1G; Sigma-Aldrich) and amphotericin B (HY-B0221; MedChemExpress) were referenced antifungal agents. MCD-1 was dissolved in sterile ultrapure water, whereas amphotericin B and fluconazole stock solutions were prepared in DMSO. The final DMSO concentration was maintained at 0.3% in all relevant wells, including the vehicle controls.

The antifungal activity of MCD-1 and amphotericin B was evaluated using a broth-microdilution procedure aligned with CLSI M27.[24] Twofold serial dilutions of each test agent were prepared in RPMI 1640 medium in sterile 96-well microplates. Each well contained 100 μL of the drug or peptide dilution and 100 μL of standardized fungal suspension.

Each plate included an untreated growth control, a medium-only sterility control and an appropriate vehicle control. *Candida albicans* SC5314 was used as the primary strain, while the remaining five strains were tested to determine the activity spectrum of MCD-1. Plates were incubated at 30 °C for 24 hours, using species-specific conditions validated by the host laboratory. The fungal suspension was prepared at approximately 2×10^4 CFU/mL and mixed in equal volume with the twofold-concentrated test-agent solutions, producing a final inoculum density of 1×10^4 CFU/mL and a final assay volume of 200 μL per well.

After incubation, fungal growth was quantified by measuring absorbance at 600 nm using an SH1M-SN microplate reader (Agilent Technologies), with medium-only wells used for background correction.

MIC_{90} was defined as the lowest concentration producing at least a 90% reduction in growth relative to the untreated control.[24] To determine the minimum fungicidal concentration, aliquots from wells at and above the MIC were plated onto drug-free Sabouraud dextrose agar.[25]

2.5 Growth-kinetics and Time-Kill assays

An overnight *Candida albicans* SC5314 culture was standardized and dispensed into sterile 96-well plates containing either the untreated control or MCD-1 at 1×MIC. Plates were incubated at

2026 S.T. Yau High School Science Award
仅用于2026丘成桐中学科学奖论文公示

30 °C, and growth was monitored for approximately 47 h by repeated measurement of OD600 using the SH1M-SN microplate reader. Growth curves and area-under-the-curve values were generated in GraphPad Prism 10.3.1.[26]

The time-dependent fungicidal activity of MCD-1 was also evaluated against *Candida albicans* SC5314 using a colony-counting assay. The starting fungal suspension contained approximately 1.9×10^6 CFU/mL, based on the viable counts recorded at time zero. Fungal suspensions were exposed to MCD-1 or amphotericin B at 1× and 2× their respective MIC values. Aliquots were collected at 0, 30, 60, 90, and 120 min, serially diluted, and plated onto drug-free YPD. Following incubation at 30°C for 48 h, viable colonies were counted and expressed as $\log_{10}$ CFU/mL. Two recorded replicates were available for each condition, and the results are presented as the mean ± SD.

2.6 Antibiofilm activity

2.6.1 Inhibition of biofilm formation

The effect of MCD-1 on biofilm establishment was quantified using crystal violet staining.[27] Standardized *Candida albicans* SC5314 suspensions were added to 96-well plates and exposed to PBS, MCD-1, or fluconazole during adhesion and early biofilm development. MCD-1 and fluconazole were tested at 1× and 2× their respective MIC values. Following incubation for 24 hours at 30 °C, nonadherent cells were removed by standardized washing with PBS.

After removal of nonadherent cells, the remaining biofilms were stained with crystal violet, washed to remove unbound dye, and the retained dye was solubilized.[27] The SH1M-SN microplate reader measured absorbance and normalized it to the untreated biofilm control.

2.6.2 Activity against mature biofilms

Nonadherent cells were removed, and the biofilms were exposed to PBS, MCD-1, or fluconazole at 1× and 2× their respective MFC values. Biofilm metabolic activity was subsequently quantified using an XTT reduction assay.[28]

An XTT working solution containing electron-coupling reagent was added to the washed biofilms. After incubation protected from light, the colored supernatant was transferred to a clean microplate and absorbance was measured using the SH1M-SN microplate reader.[28]

2.7 Checkerboard interaction assay

Interactions between MCD-1 and conventional antifungal agents were evaluated using two-dimensional broth-microdilution checkerboards.[29] Twofold serial dilutions of MCD-1 were arranged along one axis of a 96-well plate, while twofold serial dilutions of amphotericin B were arranged along the other. Each well contained 50 µL of peptide dilution, 50 µL of antifungal-drug dilution, and 100 µL of standardized fungal inoculum (final volume, 200 µL). Inoculum preparation, medium, incubation conditions, OD600 measurement using the SH1M-SN microplate reader, and endpoint determination were consistent with the single-agent MIC assay.

The fractional inhibitory concentration of each agent was calculated as:

2026 S. T. Yau High School Science Award
仅用于2026丘成桐中学科学奖公示

FIC_{pep} = MIC of MCD-1 in combination / MIC of MCD-1 alone

FIC_{drug} = MIC of drug in combination / MIC of drug alone

The fractional inhibitory concentration index was calculated as $FICI = FIC_{pep} + FIC_{drug}$. Interactions were provisionally classified as synergistic when $FICI \leq 0.5$, additive when $0.5 < FICI \leq 1$, indifferent when $1 < FICI \leq 2$ and antagonistic when $FICI > 2$.[29]

2.8 In vivo activity in *Galleria mellonella*

Final-instar *Galleria mellonella* larvae were obtained from Tianjin Huiyu Biological Technology Co., Ltd. (Tianjin, China). Healthy *Galleria mellonella* larvae weighing approximately 250 mg and showing no melanization or visible injury were randomly allocated to experimental groups of 20 larvae.[30,31] The groups comprised uninfected PBS control, uninfected peptide-only control, infected PBS control, two infected MCD-1 treatment (75 and 150 μg/mL), infected amphotericin B treatment and infected fluconazole treatment.

Candida albicans SC5314 cells were harvested from an overnight culture, washed three times with sterile PBS, and adjusted to the required concentration. Each larva received a solution of 10-μL injection through the first left proleg using a microsyringe: 2×10^5 CFU of *Candida albicans* SC5314 treated with PBS, MCD-1 (75 or 150 μg/mL), amphotericin B (2 μg/mL), or fluconazole (2 μg/mL), with the control receiving sterile PBS.[30] The larvae were maintained at 30 °C and assessed every 24 h for 7 days.[30,31]

2.9 Circular-dichroism spectroscopy

The secondary structure of MCD-1 was examined using far-UV circular-dichroism spectroscopy on an Applied Photophysics Chirascan V100 spectrometer (Applied Photophysics, UK).[32] MCD-1 was prepared at 0.2 mg/mL in ultrapure water or 50% (v/v) 2,2,2-trifluoroethanol (TFE). Spectra were recorded in a quartz cuvette with a path length of 0.5 mm at 25°C over a wavelength range of 190–260 nm.

Three consecutive scans were collected for each condition and averaged. Solvent baselines recorded under identical conditions were subtracted from the corresponding peptide spectra.[32]

2.10 Morphological and ultrastructural characterization

Scanning-electron-microscopy (SEM) and transmission-electron-microscopy (TEM) sample processing and imaging were performed by Servicebio Technology Co., Ltd. (China).

SEM images were acquired using a Hitachi SU8100 scanning electron microscope (Hitachi, Japan) at an accelerating voltage of 3.0 kV and a nominal magnification of 30,000×. TEM images were obtained using a Hitachi transmission electron microscope at an accelerating voltage of 80.0 kV and nominal magnifications of 12,000× and 40,000×.

2025 S.T. Yau High School Science Award
仅用于2026丘成桐高中科学奖论文公示

2.11 Molecular Dynamics Simulation of Peptide–Fungal Membrane Interactions

All-atom molecular dynamics (MD) simulations were performed to investigate the interaction of MCD-1 with a *Candida albicans*-mimetic membrane (CAmem). The CAmem model consisted of POPC, POPE, POPI, POPS, POPG, POPA, and DPP2 at a molar ratio of 40:27:18:7:1:6:1. All lipid molecules and the peptide were parameterized using the CHARMM36 force field.[33] The initial membrane structure and the corresponding topology files were generated using the CHARMM-GUI Membrane Builder.[34] The initial three-dimensional structure of MCD-1 (FCRSLRKLATWLLPTTFCAISKKC) was predicted using AlphaFold,[22] and its force-field topology was generated using the pdb2gmx module in GROMACS.[35]

The peptide–membrane system was placed in a periodic simulation box measuring 11 × 11 × 11 nm^3. The membrane was oriented parallel to the *xy* plane, with sufficient solvent layers included on both sides along the *z* axis. MCD-1 was initially positioned approximately 1.5 nm above the membrane surface. The system was solvated using the TIP3P water model,[36] and Na^+ or Cl^- counterions were added to neutralize the total system charge.

MD simulations were performed using GROMACS 2025.1 under periodic boundary conditions.[35] The cutoff distance for short-range nonbonded interactions was set to 1.2 nm, and long-range electrostatic interactions were calculated using the particle mesh Ewald method.[37] Following system construction, energy minimization and position-restrained equilibration were performed according to the default CHARMM-GUI protocol.[34] A 200-ns production simulation was subsequently conducted in the NPT ensemble. The temperature was maintained at 310 K using the velocity-rescaling thermostat with a coupling time constant of 1.0 ps,[38] whereas the pressure was maintained at 1 bar using the C-rescale barostat with a coupling time constant of 5.0 ps.[39] All bonds involving hydrogen atoms were constrained using the LINCS algorithm,[40] and an integration time step of 2 fs was applied.

The resulting trajectory was analyzed to characterize the peptide conformation and its association with the membrane. Analyses included peptide root-mean-square deviation (RMSD), residue-level root-mean-square fluctuation (RMSF), radius of gyration (Rg), solvent-accessible surface area (SASA), peptide–membrane hydrogen bonding, residue–lipid contacts, density distribution along the membrane-normal *z* axis, and the Gibbs free-energy landscape. A peptide residue was considered to be in contact with a membrane component when its minimum distance from that component was within 0.6 nm. Density profiles were calculated using the equilibrated 180–200 ns portion of the trajectory. The free-energy landscape was constructed using RMSD and Rg as reaction coordinates. Molecular structures and simulation snapshots were visualized using VMD.[41]

2.12 Statistical analysis

Data were analyzed using GraphPad Prism version 10.3.1.[26]

MIC and MFC results are reported as modal values and ranges across independent experiments. Differences exceeding one twofold dilution were repeated. Growth and time-kill data were analyzed using a two-way ANOVA with treatment and time as factors, followed by multiplicity-

2026 S. T. Yau High School Science Award 仅用于2026丘成桐中学科学奖文本展示

adjusted post hoc comparisons. Final-timepoint OD_{600} values in the MCD-1-treated and untreated groups were compared using a two-sided independent-samples Student's t-test assuming equal variances. Crystal-violet and XTT results were analyzed using two-way ANOVA with treatment and concentration as factors when model assumptions were satisfied.

Checkerboard results are reported as replicate-level FICI values and complete concentration–response matrices. Larval survival was analyzed using Kaplan–Meier curves[42] and prespecified log-rank tests with correction for multiple comparisons.[43]

3. Results

3.1 AI-Assisted screening identifies a promising AFP candidate

The AI-assisted generation and screening pipeline is summarized in Figure 1. Five candidate peptides, designated peptides A–E, were evaluated using the pepADMET platform. Their sequences ranged from 17 to 31 amino acids, with predicted molecular weights between 2,150.68 and 3,281.75 Da (Table 1). All five peptides were positively charged and had alkaline isoelectric points, with predicted net charges ranging from +3.374 to +5.526 and pI values ranging from 9.074 to 11.750.

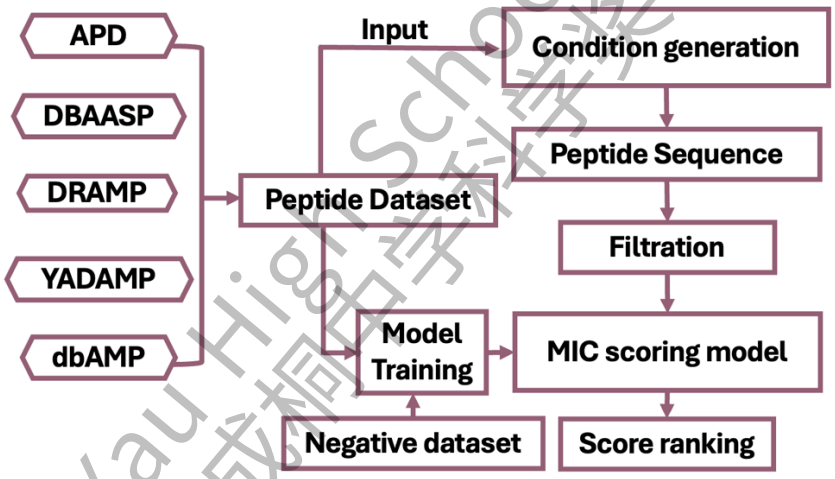


Figure 1. AI-assisted workflow for the generation and selection of MCD-1. Reference antimicrobial-peptide sequences collected from APD, DBAASP, DRAMP, YADAMP, and dbAMP were curated and supplied to the EvoGen-Pep condition model for candidate generation. A peptide dataset and a corresponding negative dataset were used to train an MIC-prediction model.[20] Generated sequences underwent sequence filtering, activity scoring, candidate ranking, and pepADMET evaluation.[21] Five candidates were shortlisted, from which MCD-1 was selected for AlphaFold 3 structural prediction and experimental validation.[22]

MCD-1 (Peptide A) exhibited the highest predicted net charge (+5.526) and hydrophobic-residue ratio (0.500) among the five candidates. However, MCD-1 also had the highest instability index (63.438), indicating a potential stability limitation that will require experimental evaluation. Peptide D had the lowest instability index (16.594) and the highest aliphatic index (114.706), whereas peptide E displayed the highest Boman index (3.602), suggesting a comparatively high potential for nonspecific protein binding.

2026 Yau High School Science Award 作品完成后学术论文公示

Table 1. Predicted physicochemical properties of the five candidate peptides.

Peptide	Sequence	MW (Da)	Charge	pI	Instability index	Aliphatic index	Boman index	Hydrophobic ratio
A	FCRSLRKLATWLLPTTFCAISKKC	2786.440	5.526	10.914	63.438	89.583	0.860	0.500
B	STFGCCCCPGWAIRRGLSLGGTRG	2457.890	3.374	9.136	40.025	52.917	1.003	0.375
C	RHHNYTCLAGNFRGPCNRHGCSLGLGLCPAG	3281.750	3.497	9.074	29.539	56.774	1.540	0.355
D	YKYCLWVIKIKLAEPRK	2150.680	4.830	10.502	16.594	114.706	0.886	0.412
E	GIRKFRLSLAQQHFQELDKLRKERP	3093.600	5.031	11.750	26.080	82.000	3.602	0.320

AlphaFold 3 predicted that MCD-1 adopts a partially α-helical conformation with comparatively flexible terminal regions (Figure 2). This model was treated as an initial structural hypothesis for subsequent CD characterization and molecular-dynamics simulation rather than as experimental evidence of the peptide's solution structure.

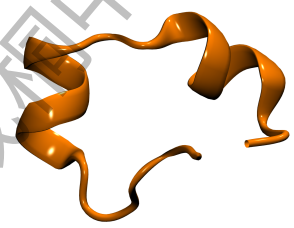


Figure 2. AlphaFold-predicted structure of MCD-1. The predicted model contains a central α-helical region together with less ordered terminal segments. The structure was used as the initial model for molecular-dynamics.

3.2 MCD-1 exhibits species- and strain-dependent antifungal activity

The antifungal activity of MCD-1 was evaluated against six fungal isolates using MIC_{90} and minimum fungicidal concentration assays. Amphotericin B was included as a reference antifungal agent. MCD-1 exhibited measurable activity against five of the six tested isolates, although its potency varied substantially among species and strains (Table 2).

2026 S.-T. Yau High School Science Award 仅用于2026丘成桐中学科学奖论文公示

The greatest susceptibility to MCD-1 was observed for *Candida tropicalis* 305, with an MIC_{90} of 4.69 µg/mL and an MFC of 18.75 µg/mL. *Candida tropicalis* 93 and *Cryptococcus* sp. 909 were also susceptible, with MIC_{90} values of 9.38 µg/mL and MFC values of 18.75 µg/mL. Intermediate activity was observed against *Candida albicans* SC5314, for which the MIC_{90} and MFC were 75 and 150 µg/mL, respectively.

MCD-1 was less active against *Cryptococcus* sp. 994, with an MIC_{90} of 150 µg/mL and an MFC of 300 µg/mL. The lowest susceptibility was observed for *Nakaseomyces glabratus* 310, for which the MIC_{90} was 300 µg/mL and the MFC exceeded the maximum concentration tested (Figure 3).

Table 2. MIC_{90} and MFC values of MCD-1 and amphotericin B against the tested fungal isolates.

Organism	Isolate number	MCD-1 MIC_{90}/MFC (µg/mL)	Amphotericin B MIC_{90}/MFC (µg/mL)
Candida albicans	SC5314	75/150	0.5/2
Candida tropicalis	93	9.38/18.75	0.5/1
Candida tropicalis	305	4.69/18.75	0.5/2
Nakaseomyces glabratus	310	300/>300	0.5/2
Cryptococcus sp.	909	9.38/18.75	0.25/0.5
Cryptococcus sp.	994	150/300	2/>32

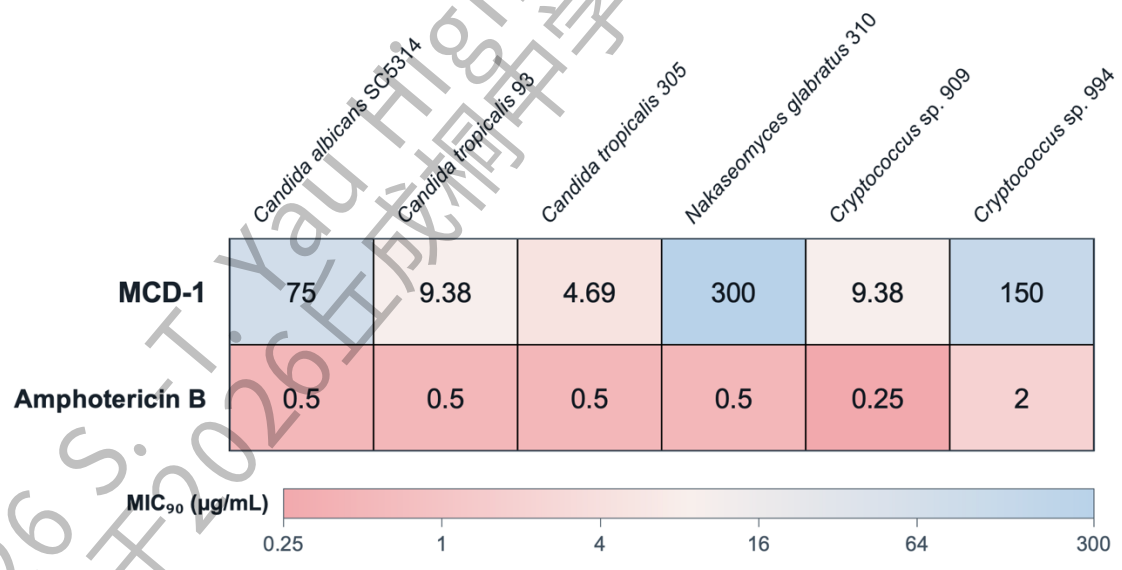


Figure 3. Antifungal susceptibility profile of MCD-1. Heatmaps showing the MIC_{90} values of MCD-1 and amphotericin B against the tested fungal isolates.

2026 S.T. Yau High School Science Award
仅用于2026丘成桐中学科学奖论文公示

3.3 MCD-1 suppresses planktonic fungal growth

The effect of MCD-1 on fungal growth kinetics was assessed over approximately 47 h. In the untreated control, the mean optical-density signal increased from approximately 0.083 at the beginning of the experiment to 1.278 at 47.24 h. Treatment with MCD-1 at 1×MIC reduced the increase in optical density, producing a mean final value of approximately 0.913. At the final time point, OD_{600} was significantly lower in the MCD-1-treated group than in the untreated control (two-sided independent-samples Student's t-test, $|t| \approx 6.34$, $df = 4$, $p \approx 0.0032$).

Analysis of the complete growth curves produced an approximate area under the curve of 33.79 for the untreated control and 17.05 for the peptide-treated group. This represented an approximately 49.5% reduction in cumulative growth following MCD-1 treatment. Nevertheless, the optical-density signal continued to increase in the peptide-treated cultures.

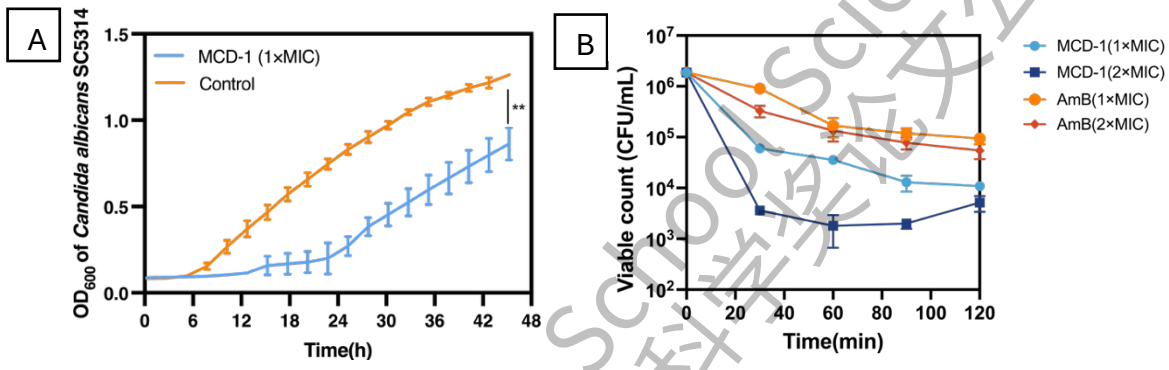


Figure 4. Effects of MCD-1 on planktonic growth and fungal viability. (A) Optical-density growth kinetics of *Candida albicans* SC5314 cultured in the absence or presence of MCD-1 at 1×MIC over approximately 47 h. Two asterisks at the final point indicate $p < 0.01$ (two-sided independent-samples Student's t-test; $p \approx 0.0032$). (B) CFU-based time-kill kinetics following exposure to MCD-1 or amphotericin B at 1× and 2×MIC for 120 min.

The CFU-based time-kill assay also demonstrated a rapid and concentration-dependent reduction in viable *Candida albicans* SC5314 following exposure to MCD-1 (Figure 4B). The mean starting fungal density was 6.27 ± 0.03 $\log_{10}$ CFU/mL. At 1×MIC, MCD-1 progressively reduced the viable count to 4.03 ± 0.04 $\log_{10}$ CFU/mL after 120 min, corresponding to a 2.24-$\log_{10}$ reduction from the initial inoculum.

MCD-1 at 2×MIC produced a more rapid decline, reducing the viable count to 3.55 ± 0.07 $\log_{10}$ CFU/mL after 30 min and 3.21 ± 0.29 $\log_{10}$ CFU/mL after 60 min. The latter represented an approximately 3.07-$\log_{10}$ reduction from the starting inoculum. Viable counts subsequently increased slightly, reaching 3.70 ± 0.15 $\log_{10}$ CFU/mL at 120 min, indicating partial regrowth and demonstrating that the ≥3-$\log_{10}$ reduction was not sustained throughout the observation period.

Under the same conditions, amphotericin B produced smaller reductions over 120 min. Viable counts reached 4.97 ± 0.10 and 4.73 ± 0.14 $\log_{10}$ CFU/mL at 1×MIC and 2×MIC, respectively, corresponding to reductions of approximately 1.30 and 1.55 $\log_{10}$.

2026 Tsinghua School Science Award 仅用于2026年清华科学奖公示

3.4 MCD-1 inhibits biofilm formation

The effect of MCD-1 on the formation of fungal biofilms was evaluated using crystal violet staining, which measures total attached biofilm biomass. Untreated biofilm biomass was normalized to approximately 100%. As shown in Figure 5, at 1×MIC, MCD-1 reduced the mean relative biomass to 15.57 ± 8.32%, corresponding to an approximately 84.4% reduction relative to the untreated control. At 2×MIC, the remaining biomass was 11.64 ± 1.48%, corresponding to an approximately 88.4% reduction.

Fluconazole produced mean relative biomass values of 15.25 ± 1.18% and 14.25 ± 3.87% at 1×MIC and 2×MIC, respectively. Thus, under the tested conditions, both MCD-1 and fluconazole strongly inhibited biofilm establishment. Increasing MCD-1 from 1×MIC to 2×MIC produced a modest additional decrease in biomass, whereas the two fluconazole concentrations generated similar responses.

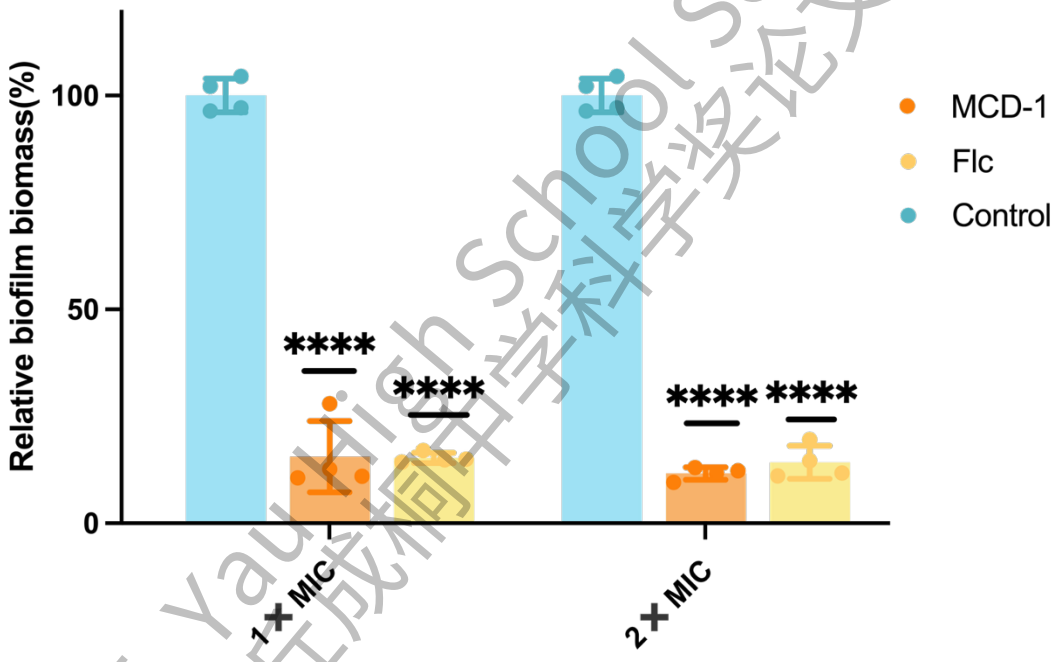


Figure 5. MCD-1 inhibits fungal biofilm formation. Biofilm formation by *Candida albicans* SC5314 was evaluated following treatment with MCD-1 or fluconazole at 1× and 2×MIC.

3.5 MCD-1 reduces the metabolic activity of mature biofilms

The activity of MCD-1 against established biofilms was evaluated using the XTT reduction assay. Unlike crystal violet staining, XTT reduction reflects the metabolic activity of viable cells within the biofilm rather than total biofilm biomass.

The untreated control displayed a mean normalized metabolic activity of 101.03 ± 20.45%. Treatment with MCD-1 at 1×MFC reduced metabolic activity to 45.29 ± 4.21%, representing an approximately 55.2% reduction relative to the control. Increasing the concentration to 2×MFC

2026 S. T. Yau High School Science Award
仅用于2026丘成桐中学科学奖论文公示

further reduced metabolic activity to 14.12 ± 5.60%, corresponding to an approximately 86.0% reduction.

Shown in Figure 6, fluconazole reduced metabolic activity to 61.32 ± 15.57% at 1×MFC and 56.91 ± 7.87% at 2×MFC, corresponding to reductions of approximately 39.3% and 43.7%, respectively. Unlike MCD-1, increasing the fluconazole concentration did not substantially increase its activity against the mature biofilm.

The existing two-way ANOVA indicated a significant overall effect of MCD-1 treatment compared with the untreated control, $F(1,12) = 91.89$, $p < 0.0001$. The concentration effect and treatment-by-concentration interaction did not reach statistical significance ($p = 0.058$ for both). Fluconazole also produced a significant overall treatment effect, $F(1,12) = 24.63$, $p = 0.0003$, whereas neither its concentration effect nor interaction was significant ($p = 0.798$ for both).

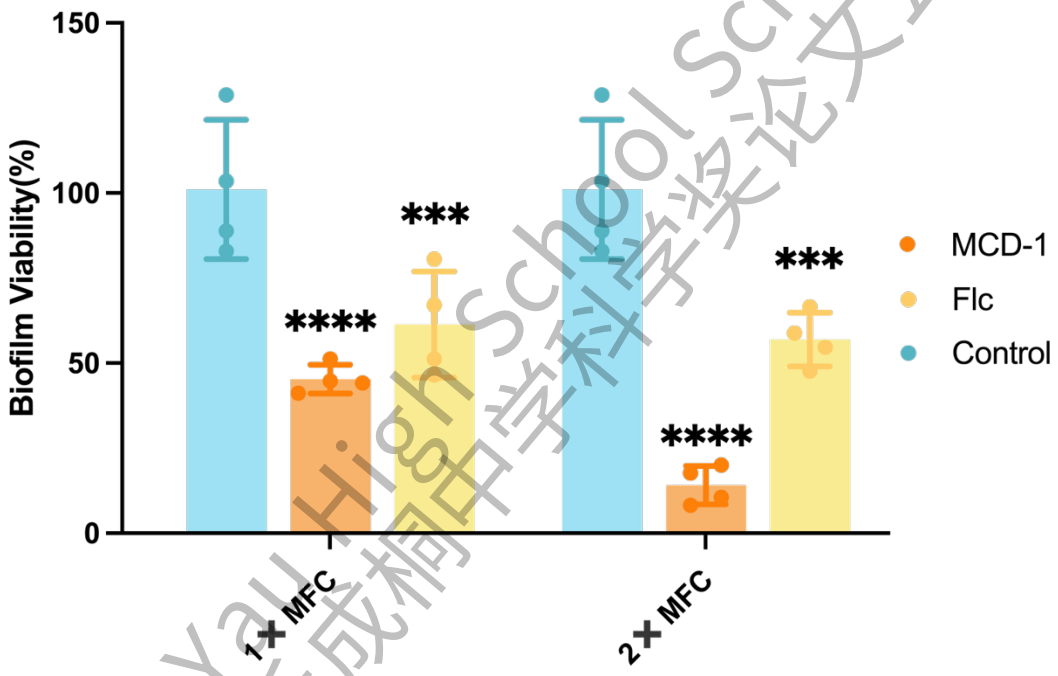


Figure 6. MCD-1 reduces the metabolic activity of mature fungal biofilms. Mature biofilms of *Candida albicans* SC5314 were treated with MCD-1 or fluconazole at 1× and 2×MFC.

3.6 Checkerboard analysis indicates a preliminary synergistic interaction between MCD-1 and amphotericin B

Checkerboard broth-microdilution analysis was used to examine the interaction between MCD-1 and amphotericin B against *Candida albicans* SC5314 (Figure 7). Within the checkerboard experiment, the single-agent MIC_{90} values were 18.75 µg/mL for MCD-1 and 1.0 µg/mL for amphotericin B.

The lowest calculated FICI was obtained with 1.17 µg/mL MCD-1 combined with 0.0625 µg/mL amphotericin B. The corresponding fractional inhibitory concentrations were 0.0625 for both

2026 Yau High School Science Award
仅用于2026年成都中学科学类论文公示

agents, producing a FICI of 0.125. This value satisfied the prespecified criterion for synergy (FICI ≤ 0.5), indicating that substantially lower concentrations of both agents inhibited fungal growth when used in combination than when used individually.

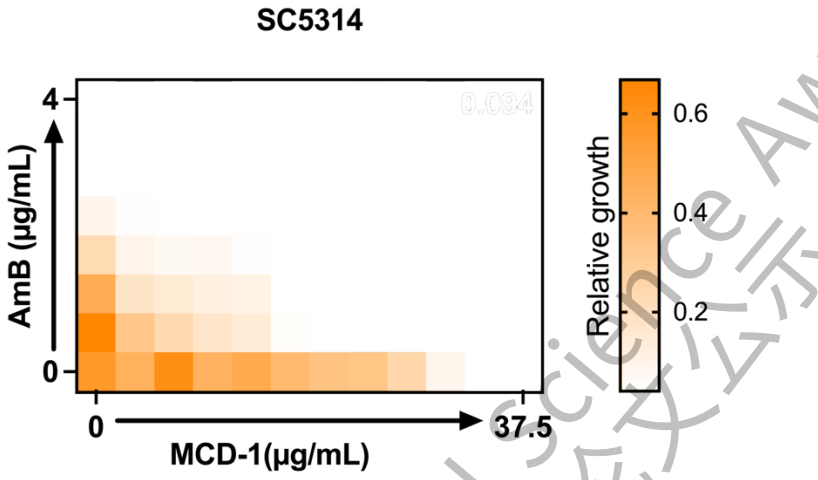


Figure 7. Checkerboard interaction between MCD-1 and amphotericin B against *Candida albicans* SC5314. The heatmap shows fungal growth across twofold concentration gradients of MCD-1 and amphotericin B.

The single-agent MIC_{90} of MCD-1 against SC5314 in the checkerboard experiment was 18.75 μg/mL, which was lower than the value reported in Table 2 (75 μg/mL). This inter-experiment variation may reflect differences in inoculum preparation, plate batch, or incubation conditions.

3.7 Circular dichroism reveals solvent-dependent conformational plasticity

The far-UV circular-dichroism spectrum of MCD-1 in water displayed a pronounced negative minimum at approximately 198 nm and lacked the characteristic double minima associated with a stable α-helical conformation (Figure 8). Secondary-structure estimation indicated that MCD-1 was predominantly unordered in water, comprising 52.7% random coil, 24.0% β-sheet, 17.6% turn, and only 5.7% α-helix (Table 3).

In 50% TFE, the CD spectrum changed markedly, displaying a positive band near 192 nm and negative bands at approximately 207 and 222 nm, consistent with increased α-helical character. The estimated α-helical content increased from 5.7% in water to 44.0% in 50% TFE, while the random-coil content decreased from 52.7% to 32.8%. The estimated β-sheet content decreased from 24.0% to 8.0%, whereas the turn content changed more modestly from 17.6% to 15.2%.

2026 S.T. Yau High School Science Award
仅用于2026丘成桐中学科学奖论文公示

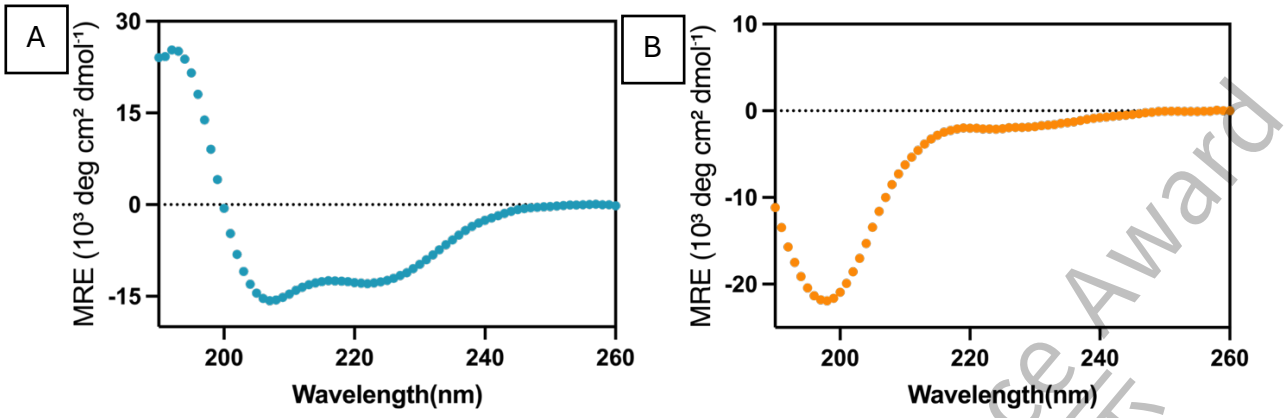


Figure 8. Solvent-dependent circular-dichroism spectra of MCD-1. A) Spectra of MCD-1 in TFE. B) Spectra of MCD-1 in water. Far-UV circular-dichroism spectra of MCD-1 recorded at 0.2 mg/mL in ultrapure water and 50% (v/v) 2,2,2-trifluoroethanol (TFE) at 25°C over 190–260 nm. MRE, mean residue ellipticity.

Table 3. Estimated secondary-structure composition of MCD-1 in water and 50% (v/v) TFE. The proportions of α-helix, β-sheet, turn, and random-coil conformations were estimated by deconvolution of the far-UV circular-dichroism spectra. Values are expressed as percentages of the total estimated secondary structure.

Secondary structure	H_2O (%)	50% TFE (%)
α-Helix	5.7	44.0
β-Sheet	24.0	8.0
Turn	17.6	15.2
Random coil	52.7	32.8
Total	100.0	100.0

3.8 MCD-1 increases survival in a *Galleria mellonella* infection model

The in vivo antifungal activity of MCD-1 was examined using *Galleria mellonella* larvae infected with *Candida albicans* SC5314. Kaplan–Meier analysis demonstrated a significant overall difference among the five survival curves (log-rank Mantel–Cox test, χ^2=17.63, df=4, P=0.0015; Figure 9). Survival in the infected control group decreased to 55% by day 3 and reached 50% at the end of the seven-day observation period.

In comparison, both the 75 and 150 μg/mL MCD-1 groups maintained 95% survival from day 3 to day 7. The final survival rates in the amphotericin B and fluconazole groups were 75% and 70%, respectively. Thus, MCD-1 treatment was associated with higher larval survival under the tested conditions.

2026 S. T. Yau High School Science Award
仅用于2026丘成桐中学科学奖论文公示

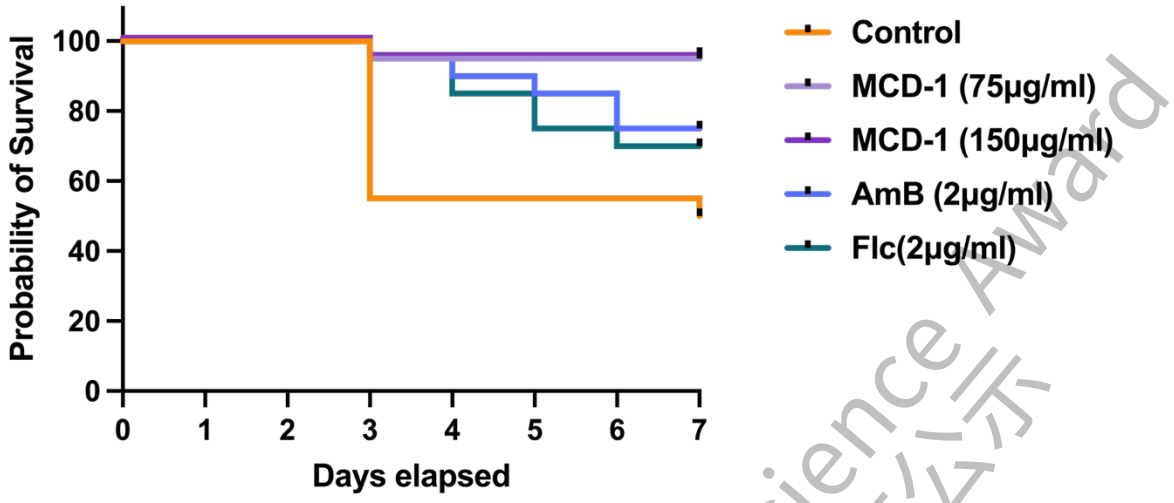


Figure 9. Effect of MCD-1 on the survival of *Candida albicans*-infected *Galleria mellonella*. Kaplan–Meier survival curves of larvae infected with 2×10^5 CFU of *Candida albicans* SC5314 per larva and treated with PBS, MCD-1 at 75 or 150 μg/mL, amphotericin B (AmB) at 2 μg/mL, or fluconazole (FLC) at 2 μg/mL. Each group contained 20 larvae, and survival was monitored for 7 days. The survival distributions differed significantly among the five groups (log-rank Mantel–Cox test, χ^2=17.63, df=4, P=0.0015).

3.9 Electron microscopy reveals peptide-induced cellular and membrane damage

Electron microscopy revealed marked morphological and ultrastructural differences between untreated and MCD-1-treated fungal cells (Figure 10). Following peptide exposure, TEM showed irregular and locally disrupted cell-envelope regions, surface-associated material, and heterogeneous intracellular electron density in the overview and enlarged detail images (Figure 10C, D). By contrast, untreated cells displayed a comparatively continuous cell envelope and preserved intracellular organization (Figure 10A, B). Consistent surface alterations were observed by SEM: untreated cells retained a relatively regular external morphology (Figure 10E), whereas peptide-treated cells showed pronounced surface depressions and irregular pit-like defects (Figure 10F). These observations support peptide-associated perturbation of the fungal cell envelope and cellular ultrastructure.

2026 S. T. Yau High School Science Award
仅用于2026丘成桐中学科学奖公示

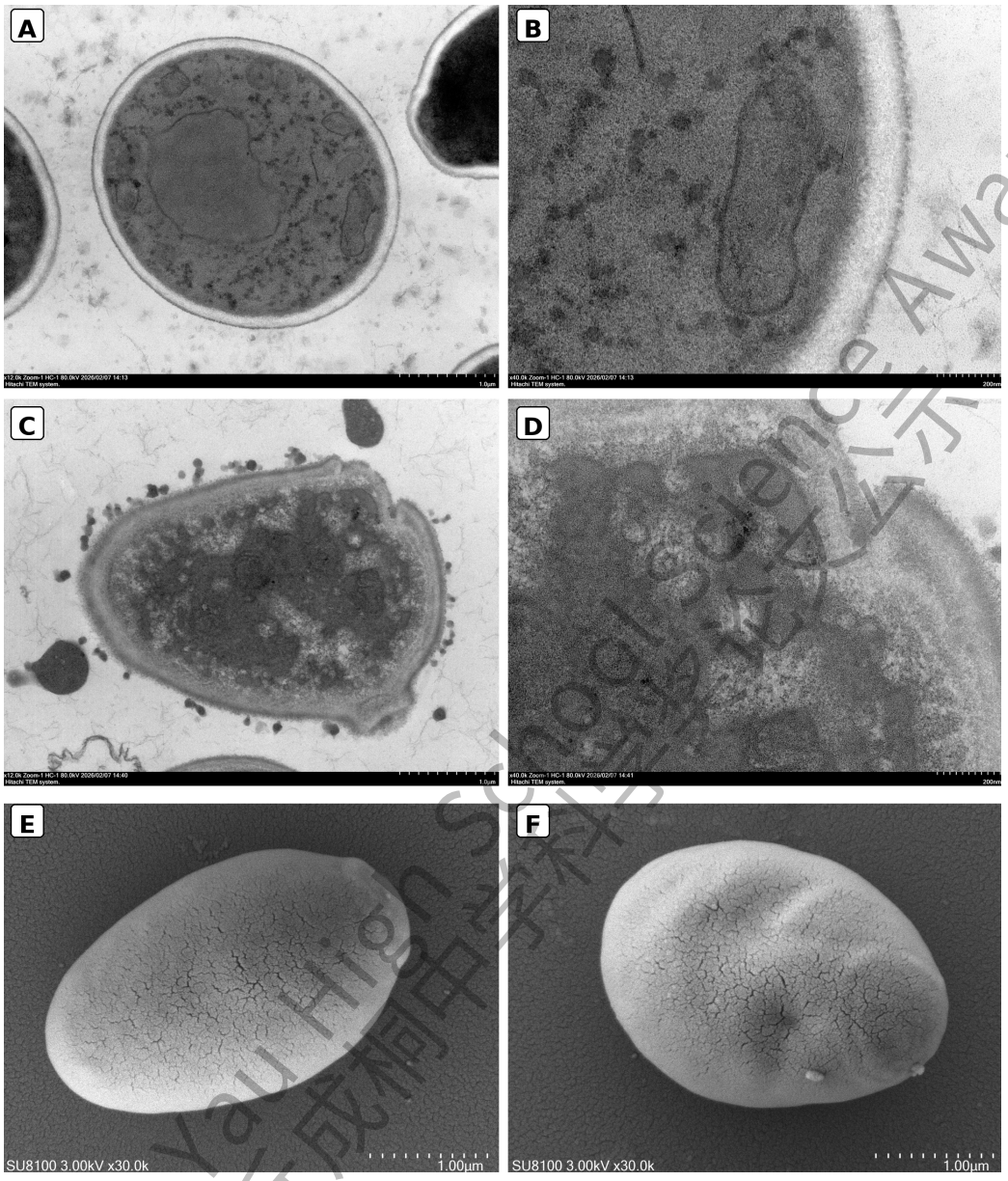


Figure 10. MCD-1-associated morphological and ultrastructural alterations in *Candida albicans* SC5314. (A) TEM overview of an untreated control cell (12,000×; scale bar, 1.0 µm). (B) Higher-magnification TEM detail of an untreated cell envelope (40,000×; scale bar, 200 nm). (C) TEM overview after MCD-1 treatment (12,000×; scale bar, 1.0 µm). (D) Higher-magnification TEM detail after MCD-1 treatment (40,000×; scale bar, 200 nm). (E) SEM image of an untreated control cell (30,000×; scale bar, 1.00 µm). (F) SEM image after MCD-1 treatment (30,000×; scale bar, 1.00 µm).

3.10 Molecular-dynamics simulations reveal persistent interfacial association of MCD-1 with a fungal-membrane model

Comparison of the initial and final configurations showed that MCD-1 approached the outer membrane leaflet and remained associated with the phospholipid headgroup region throughout

2026 Shi Yan High School Science Award 仅用于2026年成柯中学科学奖公示

the 200-ns trajectory (Figure 11). The final configuration retained a partially helical central segment, whereas both termini remained more flexible. The peptide was located mainly at the membrane–water interface and did not undergo complete transmembrane insertion.

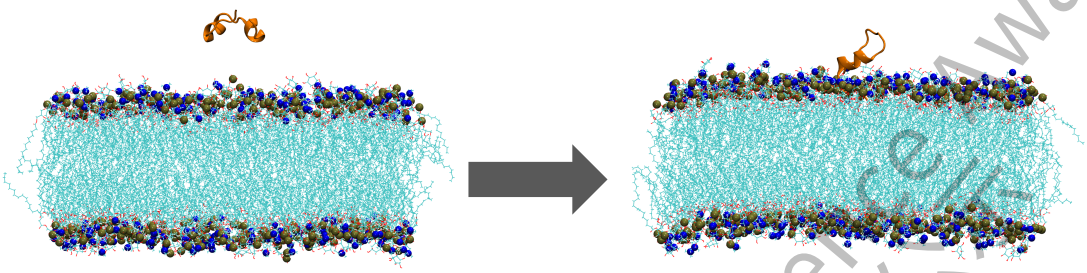


Figure 11. Initial and final configurations of MCD-1 in the *Candida albicans*-mimetic membrane system. (A) Initial configuration. (B) Configuration at 200 ns.

The backbone RMSD of MCD-1 increased during the first half of the trajectory and showed a further transient rise near the end of the 200 ns before decreasing toward the end of the simulation (Figure 12). This nonmonotonic profile indicates membrane-associated conformational rearrangement.

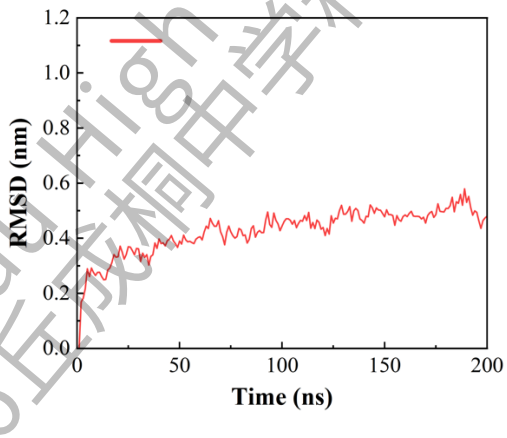


Figure 12. Backbone root-mean-square deviation (RMSD) during the 200-ns simulation.

Residue-level RMSF analysis showed that the largest fluctuations occurred at the N terminus and, to a lesser extent, at the C-terminal residues, while most residues in the central region fluctuated less (Figure 13).

2026 S. T. Yau High School Science Award
仅用于2026丘成桐中学科学奖论文公示

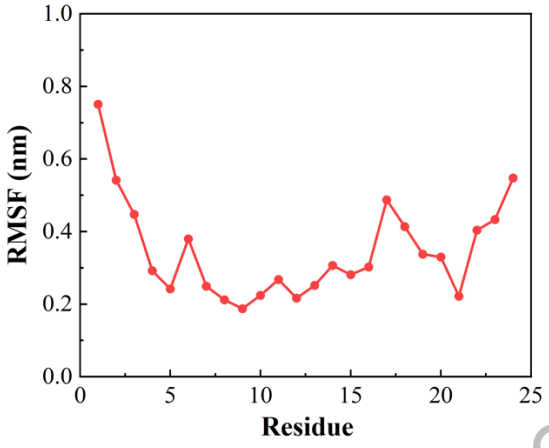


Figure 13. Per-residue root-mean-square fluctuation (RMSF).

The radius of gyration of MCD-1 fluctuated within a relatively narrow range without a sustained upward or downward trend (Figure 14). This shows that the peptide underwent local rearrangement while retaining similar overall compactness during membrane association.

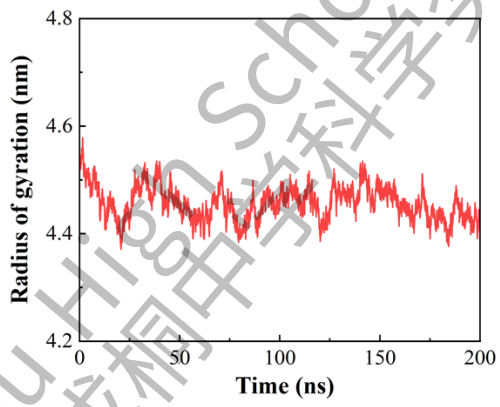


Figure 14. Radius of gyration during the simulation.

The solvent-accessible surface area (SASA) of MCD-1 initially decreased as the peptide approached the membrane, consistent with partial shielding of solvent-exposed residues (Figure 15). The later increase and continued fluctuations indicate renewed exposure of some residues as the peptide reorganized at the interface. The SASA profile therefore supports dynamic structural adaptation.

2026 S.T. Yau High School Science Award
仅用于2026丘成桐中学科学奖论文公示

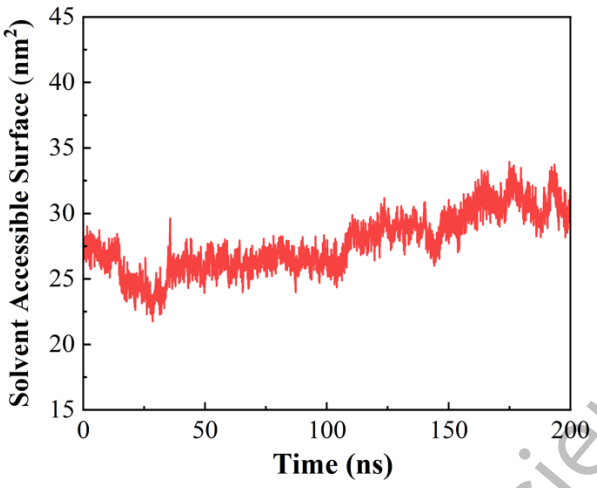


Figure 15. Solvent-accessible surface area (SASA) during the simulation.

The number of hydrogen bonds between MCD-1 and the membrane fluctuated during the early and intermediate phases and increased during the later portion of the trajectory (Figure 16). The persistence of multiple hydrogen bonds shows the progressive stabilization of polar interactions at the membrane interface.

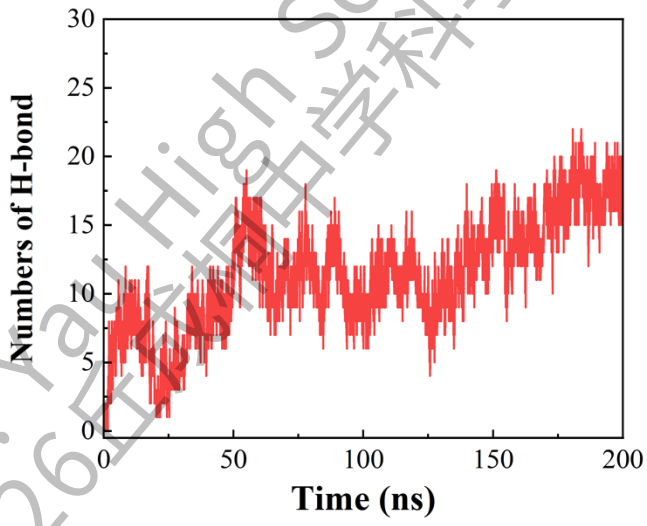


Figure 16. Hydrogen bonds between the peptide and membrane during the simulation.

Minimum-distance maps demonstrated that MCD-1 established membrane contacts early and retained multiple contacts over the complete trajectory (Figure 17). The interaction pattern shows a distributed and time-dependent interface.

2026 S. T. Yau High School Science Award
仅用于2026丘成桐中学科学奖公示

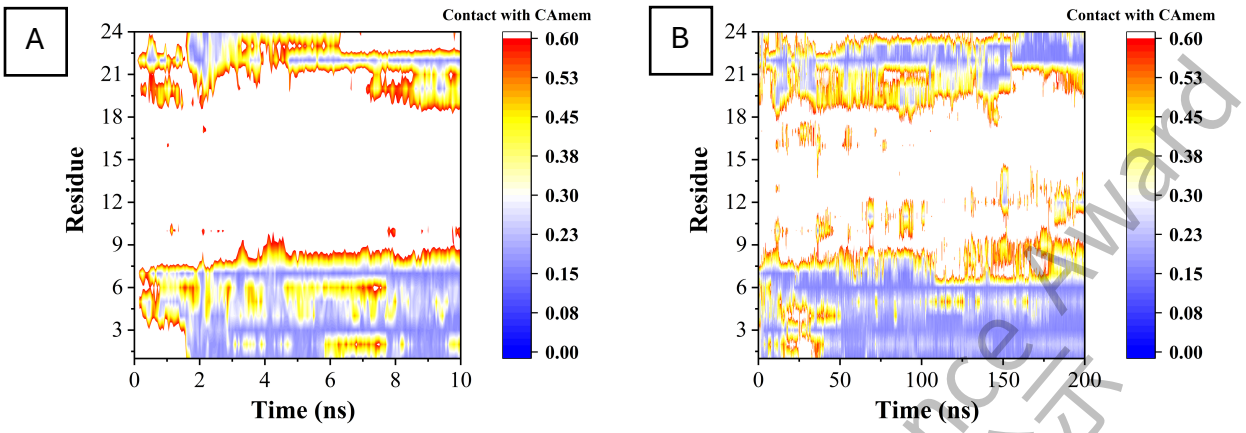


Figure 17. Minimum-distance maps for MCD-1–membrane contacts. (A) Early phase, 0–10 ns. (B) Complete trajectory, 0–200 ns.

Representative configurations identified contacts involving Phe1, Arg3, Arg6, Ser21, Lys22, and Lys23 (Figure 18). Arg3 contacted POPA, POPC, and POPE; Lys23 contacted POPS and POPC; and Arg6 and Lys22 also interacted with DPP2. The involvement of cationic Arg and Lys residues with polar or anionic lipid headgroups is consistent with an electrostatic contribution to membrane adsorption, whereas Phe1 may contribute hydrophobic anchoring at the interface.

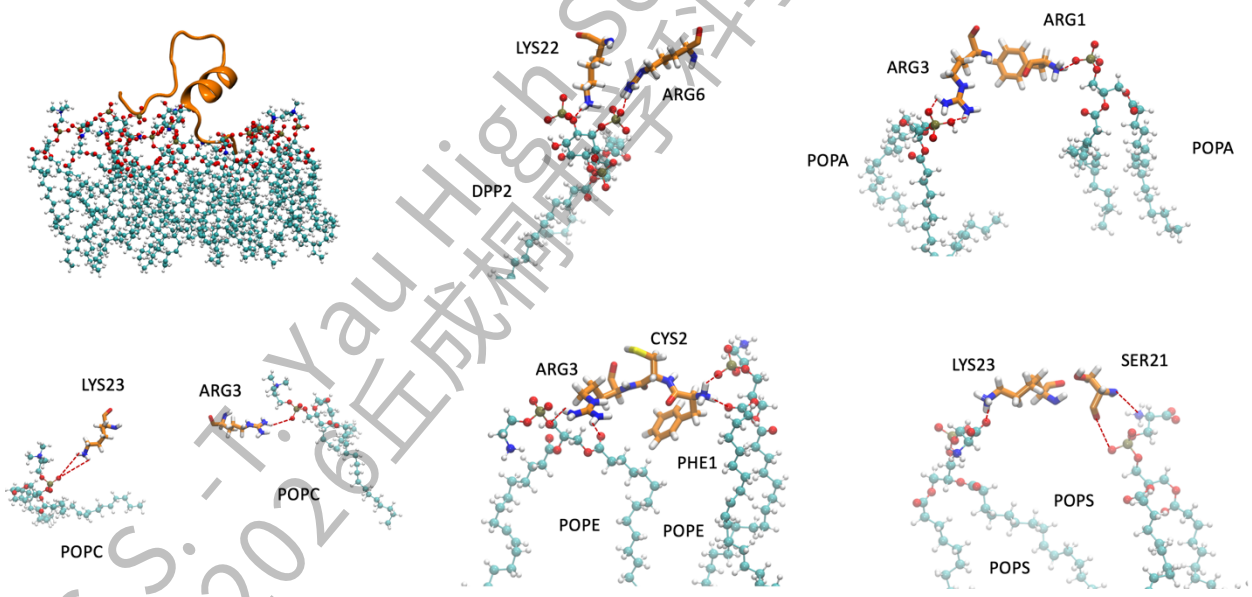


Figure 18. Representative residue–lipid interactions formed by MCD-1 during the simulation.

The density profile calculated over the final 20 ns placed MCD-1 mainly within the outer interfacial region, where its distribution overlapped with the outer phospholipid headgroups but not the complete hydrophobic core or the opposite leaflet (Figure 19). This spatial distribution supports surface adsorption and shallow interfacial association.

2026 S. T. Yau High School Science Award 仅用于2026丘成桐中学科学奖论文公示

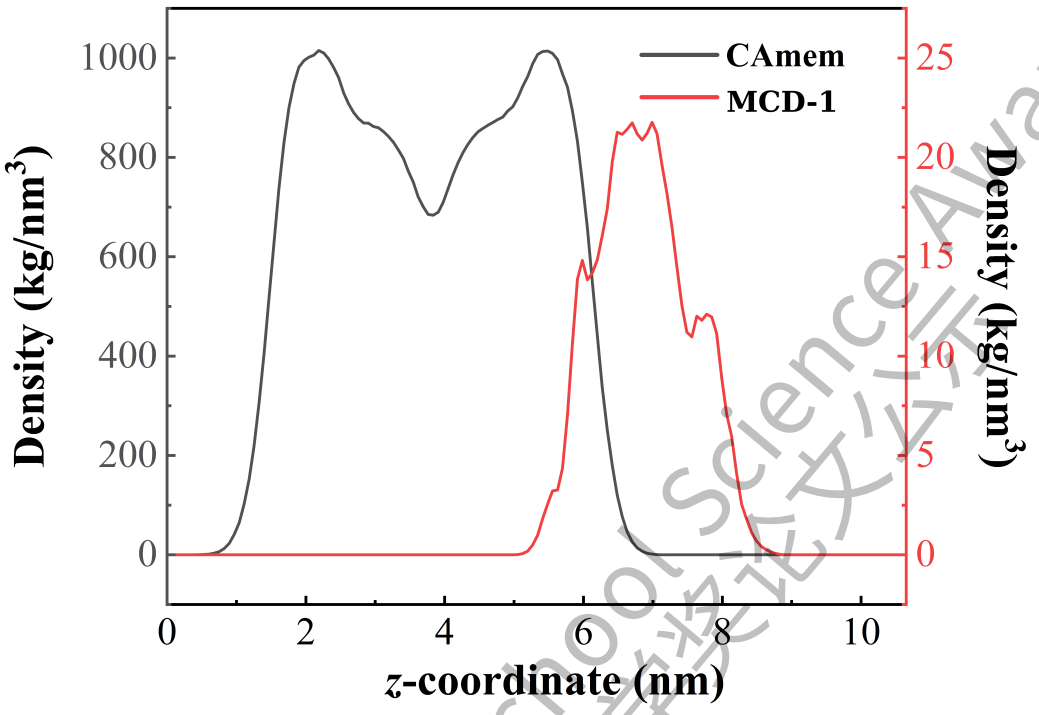


Figure 19. Number-density profile of MCD-1 and membrane components over the final 20 ns.

The Gibbs free-energy landscape contained a broad low-energy basin (Figure 20A, B). The representative low-energy configuration contained a partially helical segment together with flexible terminal regions. In combination with the RMSD, RMSF, and SASA profiles, this landscape indicates that membrane-associated MCD-1 sampled a family of related conformations.

2026 S.-T. Yau High School Science Award
仅用于2026丘成桐科学奖论文公示

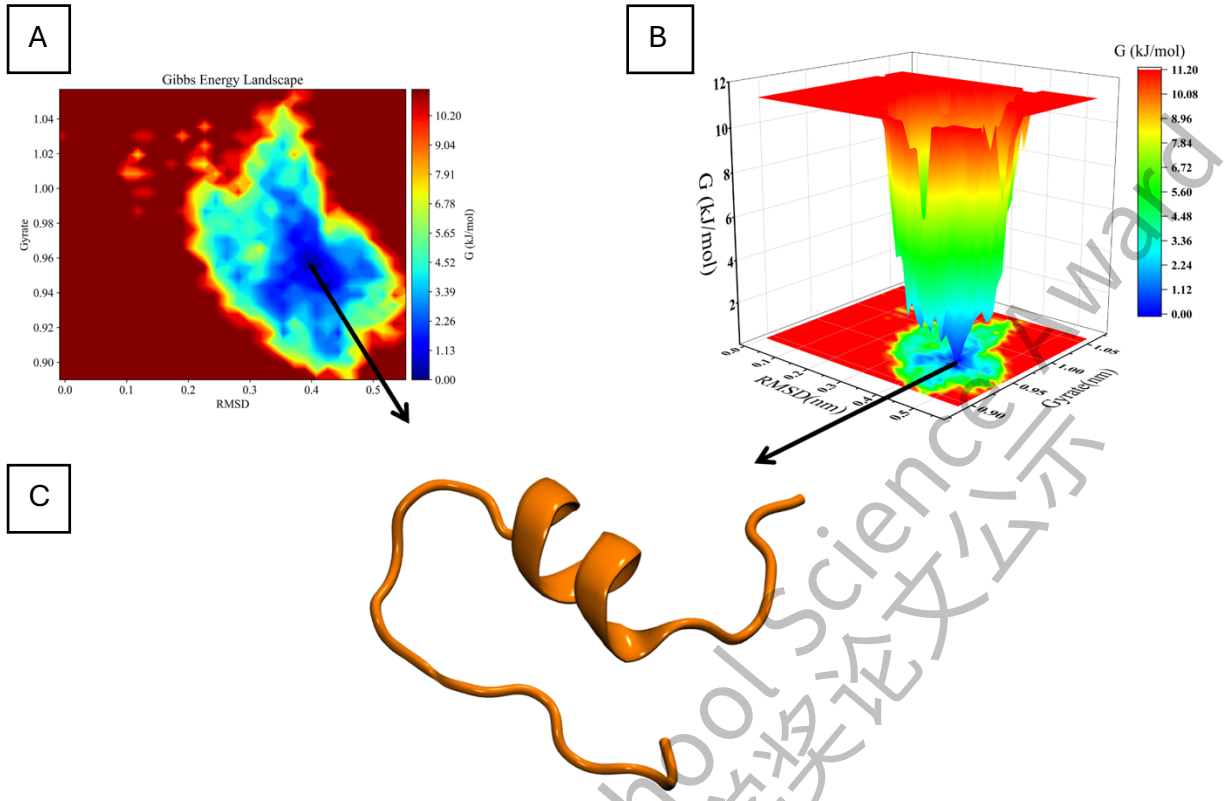


Figure 20. Free-energy landscape of membrane-associated MCD-1. (A) Two-dimensional Gibbs free-energy landscape. (B) Three-dimensional representation of the same landscape. (C) Representative conformation from a low-energy basin.

Collectively, the MD results support persistent adsorption and shallow insertion of MCD-1 at the membrane–water interface, mediated by a distributed set of cationic, polar, and hydrophobic contacts.

4. Discussion

4.1 Principal Findings

To our knowledge, this is among the first studies to combine AI-assisted antifungal peptide generation with experimental validation across planktonic growth, biofilm formation, mature biofilms, combination therapy, and an in vivo infection model, while linking phenotypic findings to membrane-interfacial mechanism.

MCD-1 (FCRSLRKLATWLLPTTFCAISKKC), designated Mycendin-1, was selected as the lead candidate because it combined the highest predicted positive charge (+5.526) and hydrophobic-residue ratio (0.500) among the five candidates. These properties are compatible with those of many membrane-interacting antimicrobial peptides.[10]

Experimental testing demonstrated that MCD-1 possessed antifungal activity, but its potency differed substantially among fungal species and strains. The peptide was most active against the two *Candida tropicalis* isolates and *Cryptococcus* sp. 909, displayed intermediate activity against *Candida albicans* SC5314, and was markedly less active against *Nakaseomyces glabratus* and *Cryptococcus* sp. 994. The results therefore support a species- and strain-dependent activity.

2026 Tianyau High School Science Award 田宇2026年成桐中学科学奖论文公示

MCD-1 also inhibited planktonic growth and displayed activity at two distinct stages of biofilm development. It strongly reduced the establishment of new biofilms and produced a concentration-associated trend toward reduced metabolic activity in mature biofilms. Mature fungal biofilms frequently exhibit substantially reduced susceptibility to conventional antifungal treatment.[9]

The *Galleria mellonella* experiment provides preliminary in vivo support for the antifungal activity of MCD-1. Both tested MCD-1 concentrations were associated with 95% survival at day 7, compared with 50% in the infected control group. The absence of separation between the 75 and 150 μg/mL curves suggests that the protective response may have reached a plateau within the tested concentration range, although additional doses and larger independently replicated experiments would be required to establish a dose–response relationship.

The amphotericin B and fluconazole groups reached final survival rates of 75% and 70%, respectively. Overall, the findings justify further evaluation of MCD-1 in vivo, including fungal-burden measurements, toxicity controls, pharmacokinetic studies, and testing in mammalian infection models.[31]

Finally, CD spectroscopy, electron microscopy, and molecular-dynamics simulation provided complementary evidence. MCD-1 showed a marked increase in α-helical content in 50% TFE, indicating environment-dependent conformational plasticity. The molecular simulation likewise showed a dynamic peptide that remained associated with the membrane headgroup region through distributed residue–lipid contacts and hydrogen bonding. SEM and TEM revealed surface depressions, pit-like defects, irregular envelope regions, and altered intracellular electron density after treatment. Together, these findings support a model in which MCD-1 associates with and perturbs the fungal cell envelope.

4.2 Antifungal and Antibiofilm Potential of the Lead Peptide

MCD-1 demonstrated measurable activity against five of the six fungal isolates included in the current susceptibility dataset. Its greatest activity was observed against *Candida tropicalis* 305, with an MIC_{90} of 4.69 μg/mL and an MFC of 18.75 μg/mL. *Candida tropicalis* 93 and *Cryptococcus* sp. 909 were also susceptible, with MIC_{90} values of 9.38 μg/mL. In contrast, the MIC_{90} against *Candida albicans* SC5314 was 75 μg/mL, while values of 150 and 300 μg/mL were obtained against *Cryptococcus* sp. 994 and *Nakaseomyces glabratus*, respectively. These differences suggest that the cellular-envelope composition, membrane-lipid organization, capsule production, peptide uptake, or stress responses of individual fungi may influence susceptibility to MCD-1.[10]

The growth-kinetic experiment further showed that MCD-1 suppressed planktonic fungal growth. Treatment at 1×MIC reduced the approximate area under the optical-density growth curve from 33.79 in the untreated control to 17.05, representing an approximately 49.5% reduction in cumulative growth. However, the optical-density signal continued to increase in the treated culture. The result demonstrates delayed or reduced growth of fungi.

MCD-1 exhibited particularly encouraging activity against fungal biofilms. During biofilm formation, treatment at 1× and 2×MIC reduced normalized biomass to 15.57 ± 8.32% and 11.64 ± 1.48%, respectively. These values corresponded to reductions of approximately 84.4% and 88.4% relative to the untreated control. Fluconazole produced similarly low biomass values

2026 S. T. Yau High School Science Award 仅用于2026丘成桐中学科学奖公示

under the tested conditions. Because crystal violet measures attached cells together with extracellular matrix, these results demonstrate reduced total biofilm biomass.[27]

MCD-1 also retained activity after biofilms had matured. Treatment at 1×MFC reduced normalized XTT activity to 45.29 ± 4.21%, while 2×MFC reduced it to 14.12 ± 5.60%. In comparison, fluconazole produced normalized activities of 61.32 ± 15.57% and 56.91 ± 7.87% at the corresponding concentrations. Thus, MCD-1 produced a greater numerical reduction in metabolic activity than fluconazole across the tested concentrations.

The results are consistent with emerging evidence that antifungal peptides can act against both planktonic fungi and biofilms.[10] The AI-generated AMP-29 was previously shown to possess selective activity against *Nakaseomyces glabratus* and efficacy in a murine infection model, demonstrating that computational generation can yield experimentally active antifungal sequences.[13] The dendritic peptide C4-3RP demonstrated activity against drug-resistant *Candida albicans* and biofilms, together with protease stability and in vivo efficacy.[11] SA-XV, a 15-residue fragment of S100A12, also acted against *Candida* and *Fusarium* through membrane interaction and intracellular effects on fungal DNA and mitochondria.[12]

Compared with these optimized peptides, MCD-1 shows how an AI-assisted screening process produced a peptide with experimentally confirmed planktonic and antibiofilm activity that can now be improved through rational sequence optimization.[13]

4.3 Potential for Combination Antifungal Therapy

The preliminary checkerboard analysis suggested that MCD-1 may enhance the activity of amphotericin B against *Candida albicans*. The lowest observed FICI was 0.125, meeting the prespecified criterion for synergy and indicating that fungal growth could be inhibited using substantially lower concentrations of both agents than were required individually. Such dose reduction may be therapeutically relevant because the clinical utility of amphotericin B is constrained by dose-dependent toxicity.[5]

The interaction could reflect complementary effects on the fungal membrane: amphotericin B binds membrane ergosterol,[44] whereas the CD, electron-microscopy, and molecular-dynamics results suggest that MCD-1 associates with the membrane interface and perturbs envelope organization.

4.4 Proposed Membrane-Disruption Mechanism

The combined structural data support an environment-responsive, membrane-associated model for MCD-1. In water, the peptide was predominantly disordered, whereas 50% TFE increased its α-helical content. TFE is a helix-promoting cosolvent rather than a complete fungal-membrane mimic,[45] so this transition demonstrates conformational propensity. The result is compatible with the partially helical, dynamically rearranging conformations observed in the membrane simulation.

In the simulation, MCD-1 approached the outer leaflet and remained near the phospholipid headgroup region. Contacts involving Arg3, Arg6, Lys22, and Lys23 support electrostatic attraction between the cationic peptide and polar or anionic lipids, while Phe1 may contribute hydrophobic anchoring.[46] The increasing peptide–membrane hydrogen-bond count further supports stabilization at the interface. RMSD, RMSF, radius of gyration, SASA, and free-energy

2026 T. Yau High School Science Award
仅用于2026年成果申请学术公示

analyses showed that this membrane-bound state remained conformationally dynamic, particularly at the termini.

The density profile placed MCD-1 primarily at the membrane–water interface and did not show complete bilayer crossing. These observations are compatible with an interfacial perturbation mechanism: the peptide first accumulates at the fungal surface, reorganizes its conformation, and forms distributed lipid contacts that could disturb local packing. The surface depressions, pit-like defects, envelope irregularities, and intracellular electron-density changes seen by SEM and TEM are consistent with downstream cell-envelope stress.

Overall, the CD, molecular-dynamics, and electron-microscopy findings support a proposed model in which MCD-1 undergoes environment-dependent conformational adaptation, accumulates at the fungal membrane interface, and perturbs local membrane organization, which may contribute to increased permeability, growth inhibition, and antibiofilm activity (Figure 21).

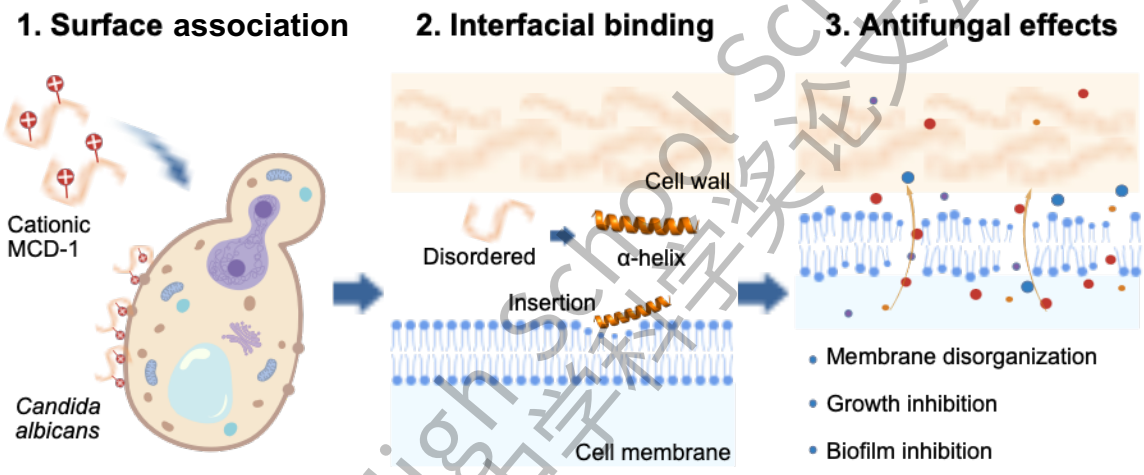


Figure 21. Proposed membrane-interaction mechanism of MCD-1. Cationic MCD-1 is proposed to associate with the fungal cell surface through electrostatic attraction, followed by environment-dependent conformational adaptation and persistent interaction with phospholipid headgroups. Surface accumulation and shallow interfacial insertion may perturb local membrane organization and increase permeability, contributing to growth and biofilm inhibition.

4.5 In Vivo Relevance

The *Galleria mellonella* experiment provides preliminary in vivo support for the antifungal activity of MCD-1. Both tested MCD-1 concentrations were associated with 95% survival at day 7, compared with 50% in the infected control group. The absence of separation between the 75 and 150 µg/mL curves suggests that the protective response may have reached a plateau within the tested concentration range.

The amphotericin B and fluconazole groups reached final survival rates of 75% and 70%, respectively. Overall, these findings provide preliminary in vivo evidence of MCD-1 activity and support its further evaluation in mammalian infection models.[31]

2026 S.T. Yau High School Science Award 仅用于2026丘成桐中学科学奖论文公示

4.6 Limitations and Future Directions

Several limitations should be considered. First, due to the limited time-span of this research, only one out of five candidates was experimentally tested. It is therefore not yet possible to determine whether the AI-assisted procedure enriched for active peptides relative to random, scrambled, or conventionally designed sequences. Future studies should synthesize additional high- and low-ranked candidates and include a composition-matched scrambled MCD-1 control.

Second, the precise molecular target of MCD-1 remains unknown, and its mechanism of action has not been fully resolved. CD spectroscopy demonstrated environment-dependent conformational adaptation, electron microscopy revealed cell-envelope and ultrastructural alterations, and molecular-dynamics simulation supported persistent association with the membrane-headgroup region. However, these findings are indirect and do not identify a specific lipid, protein, or cell-wall component as the molecular target of MCD-1. They also do not independently demonstrate pore formation, complete membrane translocation, or direct membrane permeabilization. Additional biochemical and biophysical target-validation experiments will therefore be required to distinguish direct membrane disruption from other membrane-associated or intracellular mechanisms.

Third, the in vivo evaluation was restricted to a single *Galleria mellonella* infection experiment. Although MCD-1 treatment was associated with improved larval survival, this invertebrate model cannot reproduce mammalian pharmacokinetics, immune responses, tissue distribution, or organ-specific toxicity.[31] The overlapping survival curves obtained with the two MCD-1 concentrations also precluded establishment of a dose-response relationship. These findings should therefore be interpreted as preliminary in vivo evidence rather than confirmation of therapeutic efficacy. Future studies should evaluate fungal burden, histopathology, dose-response relationships, pharmacokinetic behavior, and efficacy in an appropriate murine model of candidiasis.

Finally, the stability and mammalian safety of MCD-1 have not been established. Its cationic and hydrophobic properties may promote fungal-envelope interactions but may also increase nonspecific interactions with mammalian-cell membranes.[47] Hemolytic activity, mammalian-cell cytotoxicity, serum and protease stability, plasma half-life, salt sensitivity, maximum tolerated dose, and therapeutic index should be determined before MCD-1 can be considered for preclinical development.

2026 S. T. YAU High School Science Award
仅用于2026丘成桐中学科学奖公示

References

(1) Denning, D. W. Global incidence and mortality of severe fungal disease. *Lancet Infect. Dis.* **2024**, *24* (7), e428–e438. https://doi.org/10.1016/S1473-3099(23)00692-8

(2) World Health Organization. WHO fungal priority pathogens list to guide research, development and public health action; **2022**. https://www.who.int/publications/i/item/9789240060241

(3) Pappas, P. G.; Lionakis, M. S.; Arendrup, M. C.; Ostrosky-Zeichner, L.; Kullberg, B. J. Invasive candidiasis. *Nat. Rev. Dis. Primers* **2018**, *4*, 18026. https://doi.org/10.1038/nrdp.2018.26

(4) Lohse, M. B.; Gulati, M.; Johnson, A. D.; Nobile, C. J. Development and regulation of single- and multi-species *Candida albicans* biofilms. *Nat. Rev. Microbiol.* **2018**, *16* (1), 19–31. https://doi.org/10.1038/nrmicro.2017.107

(5) Logan, A.; Wolfe, A.; Williamson, J. C. Antifungal resistance and the role of new therapeutic agents. *Curr. Infect. Dis. Rep.* **2022**, *24* (9), 105–116. https://doi.org/10.1007/s11908-022-00782-5

(6) Lee, Y.; Robbins, N.; Cowen, L. E. Molecular mechanisms governing antifungal drug resistance. *npj Antimicrob. Resist.* **2023**, *1*, 5. https://doi.org/10.1038/s44259-023-00007-2

(7) Centers for Disease Control and Prevention. Clinical treatment of fungal diseases: Antifungals; **2024**. https://www.cdc.gov/fungal/hcp/clinical-care/index.html

(8) Cai, G.; Zhang, Z. Global surveillance of *Candida albicans*: MIC distributions, resistance patterns, and temporal trends from the Antimicrobial Testing Leadership and Surveillance program (2015–2024). *Antimicrob. Agents Chemother.* **2026**, *70*, e01617-25. https://doi.org/10.1128/aac.01617-25

(9) Silva, S.; Rodrigues, C. F.; Araújo, D.; Rodrigues, M. E.; Henriques, M. *Candida* species biofilms' antifungal resistance. *J. Fungi* **2017**, *3* (1), 8. https://doi.org/10.3390/jof3010008

(10) Fernández de Ullivarri, M.; Arbulu, S.; Garcia-Gutierrez, E.; Cotter, P. D. Antifungal peptides as therapeutic agents. *Front. Cell. Infect. Microbiol.* **2020**, *10*, 105. https://doi.org/10.3389/fcimb.2020.00105

(11) Li, G.; Chen, W.; Guan, H.; Lai, Z.; Shao, C.; Shan, A. Dendritic antifungal peptides as potent agents against drug-resistant *Candida albicans* and biofilm. *J. Med. Chem.* **2025**, *68* (3), 3373–3385. https://doi.org/10.1021/acs.jmedchem.4c02598

(12) Agarwal, R.; Biswas, K.; Agrawal, A.; Shankar, N. N.; Kundu, S.; Roy, D.; Son, D.; Harikishore, A.; Yennamalli, R. M.; Lee, D.; Bhunia, A.; Roy, S. SA-XV, a 15-amino acid fragment of host defense peptide S100A12, targets mitochondria and is protective against fungal infections. *J. Biol. Chem.* **2025**, *301* (10), 110743. https://doi.org/10.1016/j.jbc.2025.110743

(13) Wang, Y.; Song, M.; Liu, F.; Liang, Z.; Hong, R.; Dong, Y.; Luan, H.; Fu, X.; Yuan, W.; Fang, W.; Li, G.; Lou, H.; Chang, W. Artificial intelligence using a latent diffusion model enables the generation of diverse and potent antimicrobial peptides. *Sci. Adv.* **2025**, *11* (6), eadp7171. https://doi.org/10.1126/sciadv.adp7171

(14) Wang, G.; Li, X.; Wang, Z. APD3: The antimicrobial peptide database as a tool for research and education. *Nucleic Acids Res.* **2016**, *44* (D1), D1087–D1093. https://doi.org/10.1093/nar/gkv1278

(15) Pirtskhalava, M.; Amstrong, A. A.; Grigolava, M.; Chubinidze, M.; Alimbarashvili, E.; Vishnepolsky, B.; Gabrielian, A.; Rosenthal, A.; Hurt, D. E.; Tartakovsky, M. DBAASP v3: Database of antimicrobial/cytotoxic activity and structure of peptides as a resource for development of new therapeutics. *Nucleic Acids Res.* **2021**, *49* (D1), D288–D297. https://doi.org/10.1093/nar/gkaa991

2026 School Science Award 仅用于2026校园科学奖论文公示

(16) Shi, G.; Kang, X.; Dong, F.; Liu, Y.; Zhu, N.; Hu, Y.; Xu, H.; Lao, X.; Zheng, H. DRAMP 3.0: An enhanced comprehensive data repository of antimicrobial peptides. *Nucleic Acids Res.* **2022**, *50* (D1), D488–D496. https://doi.org/10.1093/nar/gkab651

(17) Piotto, S. P.; Sessa, L.; Concilio, S.; Iannelli, P. YADAMP: Yet another database of antimicrobial peptides. *Int. J. Antimicrob. Agents* **2012**, *39* (4), 346–351. https://doi.org/10.1016/j.ijantimicag.2011.12.003

(18) Jhong, J.-H.; Chi, Y.-H.; Li, W.-C.; Lin, T.-H.; Huang, K.-Y.; Lee, T.-Y. dbAMP: An integrated resource for exploring antimicrobial peptides with functional activities and physicochemical properties on transcriptome and proteome data. *Nucleic Acids Res.* **2019**, *47* (D1), D285–D297. https://doi.org/10.1093/nar/gky1048

(19) EvoGen-Pep. EvoGen-Pep peptide generation platform. Zhejiang University; **2025**. https://lz-evogenpep.zju.edu.cn/

(20) Hochreiter, S.; Schmidhuber, J. Long short-term memory. *Neural Comput.* **1997**, *9* (8), 1735–1780. https://doi.org/10.1162/neco.1997.9.8.1735

(21) Tan, X.; Liu, Q.; Zhou, M.; Fang, Y.; Ouyang, D.; Zeng, W.; Dong, J. pepADMET: A novel computational platform for systematic ADMET evaluation of peptides. *J. Chem. Inf. Model.* **2026**, *66* (2), 936–946. https://doi.org/10.1021/acs.jcim.5c02518

(22) Abramson, J.; Adler, J.; Dunger, J.; Evans, R.; Green, T.; Pritzel, A.; Ronneberger, O.; Willmore, L.; Ballard, A. J.; Bambrick, J.; Bodenstein, S. W.; Evans, D. A.; Hung, C.-C.; O'Neill, M.; Reiman, D.; Tunyasuvunakool, K.; Wu, Z.; Žemgulytė, A.; Arvaniti, E.; Jumper, J. M. Accurate structure prediction of biomolecular interactions with AlphaFold 3. *Nature* **2024**, *630* (8016), 493–500. https://doi.org/10.1038/s41586-024-07487-w

(23) Merrifield, R. B. Solid phase peptide synthesis. I. The synthesis of a tetrapeptide. *J. Am. Chem. Soc.* **1963**, *85* (14), 2149–2154. https://doi.org/10.1021/ja00897a025

(24) Clinical and Laboratory Standards Institute. Reference method for broth dilution antifungal susceptibility testing of yeasts (4th ed.; CLSI standard M27); **2017**.

(25) Cantón, E.; Pemán, J.; Viudes, A.; Quindós, G.; Gobernado, M.; Espinel-Ingroff, A. Minimum fungicidal concentrations of amphotericin B for bloodstream *Candida* species. *Diagn. Microbiol. Infect. Dis.* **2003**, *45* (3), 203–206. https://doi.org/10.1016/S0732-8893(02)00525-4

(26) GraphPad Software. GraphPad Prism (Version 10.3.1) ; **2024**. https://www.graphpad.com/

(27) Peeters, E.; Nelis, H. J.; Coenye, T. Comparison of multiple methods for quantification of microbial biofilms grown in microtiter plates. *J. Microbiol. Methods* **2008**, *72* (2), 157–165. https://doi.org/10.1016/j.mimet.2007.11.010

(28) Ramage, G.; Vande Walle, K.; Wickes, B. L.; López-Ribot, J. L. Standardized method for in vitro antifungal susceptibility testing of *Candida albicans* biofilms. *Antimicrob. Agents Chemother.* **2001**, *45* (9), 2475–2479. https://doi.org/10.1128/AAC.45.9.2475-2479.2001

(29) Odds, F. C. Synergy, antagonism, and what the chequerboard puts between them. *J. Antimicrob. Chemother.* **2003**, *52* (1), 1. https://doi.org/10.1093/jac/dkg301

(30) Fuchs, B. B.; O'Brien, E.; El Khoury, J. B.; Mylonakis, E. Methods for using *Galleria mellonella* as a model host to study fungal pathogenesis. *Virulence* **2010**, *1* (6), 475–482. https://doi.org/10.4161/viru.1.6.12985

(31) Giammarino, A.; Bellucci, N.; Angiolella, L. *Galleria mellonella* as a model for the study of fungal pathogens: Advantages and disadvantages. *Pathogens* **2024**, *13* (3), 233. https://doi.org/10.3390/pathogens13030233

2026 Yau Hee School Science Award 仅用于2026年比赛中学科学论文公开

(32) Kelly, S. M.; Jess, T. J.; Price, N. C. How to study proteins by circular dichroism. *Biochim. Biophys. Acta, Proteins Proteomics* **2005**, *1751* (2), 119–139. https://doi.org/10.1016/j.bbapap.2005.06.005

(33) Klauda, J. B.; Venable, R. M.; Freites, J. A.; O'Connor, J. W.; Tobias, D. J.; Mondragon-Ramirez, C.; Vorobyov, I.; MacKerell, A. D., Jr.; Pastor, R. W. Update of the CHARMM all-atom additive force field for lipids: Validation on six lipid types. *J. Phys. Chem. B* **2010**, *114* (23), 7830–7843. https://doi.org/10.1021/jp101759q

(34) Wu, E. L.; Cheng, X.; Jo, S.; Rui, H.; Song, K. C.; Dávila-Contreras, E. M.; Qi, Y.; Lee, J.; Monje-Galvan, V.; Venable, R. M.; Klauda, J. B.; Im, W. CHARMM-GUI Membrane Builder toward realistic biological membrane simulations. *J. Comput. Chem.* **2014**, *35* (27), 1997–2004. https://doi.org/10.1002/jcc.23702

(35) GROMACS development team. GROMACS 2025.1 manual. Zenodo; **2025**. https://doi.org/10.5281/zenodo.15006631

(36) Jorgensen, W. L.; Chandrasekhar, J.; Madura, J. D.; Impey, R. W.; Klein, M. L. Comparison of simple potential functions for simulating liquid water. *J. Chem. Phys.* **1983**, *79* (2), 926–935. https://doi.org/10.1063/1.445869

(37) Darden, T.; York, D.; Pedersen, L. Particle mesh Ewald: An N·log(N) method for Ewald sums in large systems. *J. Chem. Phys.* **1993**, *98* (12), 10089–10092. https://doi.org/10.1063/1.464397

(38) Bussi, G.; Donadio, D.; Parrinello, M. Canonical sampling through velocity rescaling. *J. Chem. Phys.* **2007**, *126* (1), 014101. https://doi.org/10.1063/1.2408420

(39) Bernetti, M.; Bussi, G. Pressure control using stochastic cell rescaling. *J. Chem. Phys.* **2020**, *153* (11), 114107. https://doi.org/10.1063/5.0020514

(40) Hess, B.; Bekker, H.; Berendsen, H. J. C.; Fraaije, J. G. E. M. LINCS: A linear constraint solver for molecular simulations. *J. Comput. Chem.* **1997**, *18* (12), 1463–1472. https://doi.org/10.1002/(SICI)1096-987X(199709)18:12%3C1463::AID-JCC4%3E3.0.CO;2-H

(41) Humphrey, W.; Dalke, A.; Schulten, K. VMD: Visual molecular dynamics. *J. Mol. Graphics* **1996**, *14* (1), 33–38. https://doi.org/10.1016/0263-7855(96)00018-5

(42) Kaplan, E. L.; Meier, P. Nonparametric estimation from incomplete observations. *J. Am. Stat. Assoc.* **1958**, *53* (282), 457–481. https://doi.org/10.1080/01621459.1958.10501452

(43) Mantel, N. Evaluation of survival data and two new rank order statistics arising in its consideration. *Cancer Chemother. Rep.* **1966**, *50* (3), 163–170.

(44) Gray, K. C.; Palacios, D. S.; Dailey, I.; Endo, M. M.; Uno, B. E.; Wilcock, B. C.; Burke, M. D. Amphotericin primarily kills yeast by simply binding ergosterol. *Proc. Natl. Acad. Sci. U.S.A.* **2012**, *109* (7), 2234–2239. https://doi.org/10.1073/pnas.1117280109

(45) Roccatano, D.; Colombo, G.; Fioroni, M.; Mark, A. E. Mechanism by which 2,2,2-trifluoroethanol/water mixtures stabilize secondary-structure formation in peptides: A molecular dynamics study. *Proc. Natl. Acad. Sci. U.S.A.* **2002**, *99* (19), 12179–12184. https://doi.org/10.1073/pnas.182199699

(46) Yeaman, M. R.; Yount, N. Y. Mechanisms of antimicrobial peptide action and resistance. *Pharmacol. Rev.* **2003**, *55* (1), 27–55. https://doi.org/10.1124/pr.55.1.2

(47) Chen, Y.; Mant, C. T.; Farmer, S. W.; Hancock, R. E. W.; Vasil, M. L.; Hodges, R. S. Rational design of α-helical antimicrobial peptides with enhanced activities and specificity/therapeutic index. *J. Biol. Chem.* **2005**, *280* (13), 12316–12329. https://doi.org/10.1074/jbc.M413406200

2026 年 Yau Hing Chong Science Award 仅用于 2026 年度科学论文公示

Acknowledgements

I was first drawn to fungi because they seemed to trouble some of the categories through which we ordinarily understand living things. A fungal cell can exist planktonically as an apparently discrete individual, yet under different conditions cells assemble into biofilms whose properties emerge from relations among many organisms. They act as a sort of symbol that blurs the boundaries between identity and relation. The more I read, the more I became fascinated by this form of life that challenges traditional structures of understanding life. The same goes for pathogenic fungi, as they inhabit another kind of boundary: they are eukaryotes like us, yet must somehow be selectively attacked without harming the human cells they infect. Compared with antibacterial medicine, the therapeutic possibilities remain strikingly limited. I therefore began to wonder whether an antifungal molecule could interact with the fungal cell differently from existing drugs, particularly by exploiting the physical and chemical properties of its surface and membrane. That question led me to antifungal peptides and, ultimately, to the project described in this paper.

This research was conducted under the guidance of Professor Changbin Chen at the Shanghai Institute of Materia Medica, Chinese Academy of Sciences (SIMM, CAS). I am deeply grateful to my mentor and to graduate student Xinmeng Peng for their guidance, patience, and support throughout the research process. Through discussions with my mentors, I developed the laboratory's broader research direction on pathogenic fungal infections and host immunity into a focused investigation of whether the computationally identified peptide MCD-1 possessed reproducible antifungal, antibiofilm, combination, and preliminary in vivo activity, and whether the experimental and computational evidence could support a plausible membrane-associated mechanism. All supervision and research guidance were provided without compensation.

I took primary responsibility for developing and implementing the experimental-validation strategy. With methodological advice from my mentors, I participated in selecting and adapting the assays, controls, treatment concentrations, incubation conditions, and experimental endpoints used to evaluate MCD-1. I primarily performed the fungal culture and inoculum preparation, broth-microdilution susceptibility testing, growth-kinetics and CFU-based time-kill assays, crystal-violet and XTT biofilm experiments, checkerboard interaction assays, and the *Galleria mellonella* infection experiment. Xinmeng Peng provided training in laboratory techniques, guidance on protocol implementation, and assistance with troubleshooting.

Beyond carrying out established procedures, I also monitored sources of experimental variation, repeated experiments when results were inconsistent, compared findings across independent experimental runs, and examined whether differences arose from biological effects or technical factors such as fungal growth state, inoculum density, dilution accuracy, washing, incubation time, and plate handling. I also evaluated the limitations of individual assays. For example, I distinguished optical-density growth kinetics from viable-cell time-kill measurements, recognized the partial regrowth observed during the time-kill experiment, and interpreted crystal-violet and XTT results according to the different biological properties measured by the two assays.

I took primary responsibility for organizing and analyzing the experimental data, producing and refining graphs and tables, checking numerical consistency across the manuscript, and interpreting the findings in relation to the research question. A central original contribution of my work was the integration of results obtained at different levels and bringing them together to construct a membrane-interaction hypothesis.

The computational peptide-generation framework, including AI-assisted candidate generation, activity prediction, physicochemical screening, and structural prediction, was supplied through the laboratory and my mentor. The molecular-dynamics simulation of MCD-1 interacting with a *Candida albicans*-mimetic membrane was also conducted using computational resources and guidance provided by my mentor.

Several additional components of the study involved specialized external technical assistance. MCD-1 was chemically synthesized by GenScript, with peptide purity and molecular mass assessed by HPLC and mass spectrometry. SEM and TEM sample processing and imaging were performed by Servicebio Technology Co., Ltd.

2026 Siyuan High School Science Award
仅用于2026年思源中学科学奖公示

One of the most significant challenges during the project was experimental reproducibility. Biological experiments often depended on multiple variables simultaneously, and relatively small variations in fungal growth state, starting cell density, dilution accuracy, incubation conditions, plate handling, or timing could affect the final results. Biofilm-related experiments were particularly sensitive because differences during adhesion, washing, staining, or metabolic measurement could introduce substantial variation. As a result, some experiments did not work reliably on the first attempt and had to be repeated several times. I learned to identify possible sources of variability, repeat experiments under more tightly controlled conditions, compare results across independent runs, and distinguish biological effects from technical variation.

Another difficulty was that different experimental approaches did not always produce perfectly identical or straightforward results. For example, the time-kill experiment showed a strong early reduction in viable cells at the higher MCD-1 concentration, followed by some regrowth later in the observation period. More broadly, differences between experimental batches and assay formats required repeated checking of concentrations, controls, and experimental conditions instead of assuming that every numerical result should be directly interchangeable. These experiences were an important part of learning that biological research often produces variability and unexpected results, and that the appropriate response is to investigate and report those limitations.

Time and resource limitations also shaped the project. Although five computationally shortlisted peptides were identified, only MCD-1 could undergo extensive experimental validation. This limitation helped shape the proposed future directions of the project and reinforced the distinction between identifying one promising candidate and validating the broader effectiveness of the design pipeline.

I was responsible for preparing and revising the research report, organizing the results into a coherent manuscript, integrating experimental and computational findings, preparing or refining figures and captions, and revising the discussion in response to feedback from my mentor and other researchers. My mentor reviewed drafts of the manuscript and provided feedback.

Artificial-intelligence tools were used as part of the research methodology, including EvoGen-Pep condition model for candidate generation, pepADMET for computational screening, and AlphaFold 3 for structural prediction. These computational components were supplied or conducted under my mentor's guidance, as described above. These tools were not used for laboratory experimental design, data analysis, figure preparation, or manuscript writing.

- EvoGen-Pep (Zhejiang University, 2025 version): used in May 2026 for candidate antifungal peptide sequence generation.
- pepADMET (2026 version): used in May 2026 for physicochemical property, toxicity, and hemolysis prediction.
- AlphaFold 3 (2024 version): used in June 2026 for three-dimensional structure prediction of MCD-1.

I am especially grateful to Professor Changbin Chen for providing the research opportunity, laboratory resources, scientific direction, and critical feedback. I am also deeply grateful to Xinmeng Peng for patient experimental training and troubleshooting assistance. I also thank my teacher Zhenchao Ruan for her guidance on essay writing, organization, and language refinement and the other members of the laboratory who provided technical assistance and constructive suggestions throughout the project.

Finally, I am grateful to my family and friends for tolerating the disproportionate amount of my life that gradually became occupied by fungi, peptides, failed plots, and daily laboratory visits. I began this project wanting to discover how to put antifungal peptides to meaningful use and I finish it with considerably more questions than I began with: questions about mechanisms, susceptibility, and redesigning them. I have come to think that this is probably the more meaningful outcome.

2026 S.T. Yau High School Science Award
仅用于2026年成师中学科学论文公示